

# Zinc(II) Complexes with Triplet Charge-Transfer Excited States Enabling Energy-Transfer Catalysis, Photoinduced Electron Transfer, and Upconversion

Jasmin A. Kübler, Björn Pfund, and Oliver S. Wenger\*

Cite This: *JACS Au* 2022, 2, 2367–2380

Read Online

ACCESS |



Metrics &amp; More



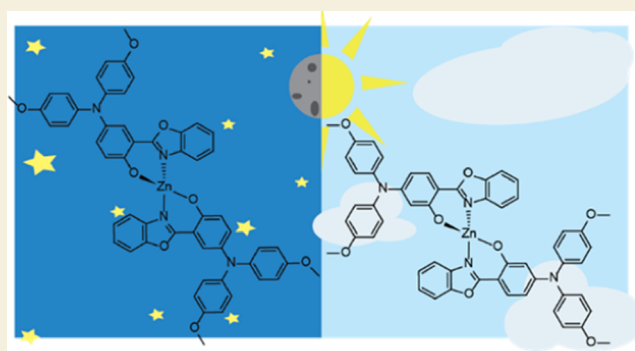
Article Recommendations



Supporting Information

**ABSTRACT:** Many  $\text{Cu}^{\text{I}}$  complexes have luminescent triplet charge-transfer excited states with diverse applications in photo-physics and photochemistry, but for isoelectronic  $\text{Zn}^{\text{II}}$  compounds, this behavior is much less common, and they typically only show ligand-based fluorescence from singlet  $\pi-\pi^*$  states. We report two closely related tetrahedral  $\text{Zn}^{\text{II}}$  compounds, in which intersystem crossing occurs with appreciable quantum yields and leads to the population of triplet excited states with intraligand charge-transfer (ILCT) character. In addition to showing fluorescence from their initially excited  $^1\text{ILCT}$  states, these new compounds therefore undergo triplet–triplet energy transfer (TTET) from their  $^3\text{ILCT}$  states and consequently can act as sensitizers for photo-isomerization reactions and triplet–triplet annihilation upconversion from the blue to the ultraviolet spectral range. The photoactive  $^3\text{ILCT}$  state furthermore facilitates photoinduced electron transfer. Collectively, our findings demonstrate that mononuclear  $\text{Zn}^{\text{II}}$  compounds with photophysical and photochemical properties reminiscent of well-known  $\text{Cu}^{\text{I}}$  complexes are accessible with suitable ligands and that they are potentially amenable to many different applications. Our insights seem relevant in the greater context of obtaining photoactive compounds based on abundant transition metals, complementing well-known precious-metal-based luminophores and photosensitizers.

**KEYWORDS:** first-row transition-metal complexes, earth-abundant metals, coordination chemistry, photocatalysis, spectroscopy



## INTRODUCTION

Tetrahedral copper(I) complexes with luminescent and redox-active metal-to-ligand charge-transfer (MLCT) excited states have long been known<sup>1,2</sup> and nowadays represent a well-developed compound class with applications in light-emitting devices,<sup>3–7</sup> dye-sensitized solar cells,<sup>8</sup> and photocatalysis.<sup>9–16</sup> In the  $3d^{10}$  valence electron configuration of  $\text{Cu}^{\text{I}}$ , there are no metal-centered (MC) excited states that can depopulate the photoactive  $^3\text{MLCT}$  states,<sup>17,18</sup> unlike for analogous  $3d^6$  ( $\text{Co}^{\text{III}}$ ,  $\text{Fe}^{\text{II}}$ ,  $\text{Mn}^{\text{I}}$ ,  $\text{Cr}^0$ )<sup>19–25</sup> or  $3d^8$  ( $\text{Ni}^{\text{II}}$ ) compounds,<sup>26,27</sup> in which nonradiative MLCT deactivation by MC states can be undesirably fast.<sup>28</sup> Consequently, complexes with the  $3d^{10}$  configuration are predisposed for obtaining long-lived and strongly emissive excited states, as illustrated for example by recently reported linear two-coordinate  $\text{Cu}^{\text{I}}$  compounds with exceptionally strongly luminescent ligand-to-ligand charge-transfer (LLCT) excited states.<sup>29–33</sup>

Isoelectronic  $\text{Zn}^{\text{II}}$  compounds have received less attention, presumably for several reasons. The higher oxidation state of  $\text{Zn}^{\text{II}}$  relative to  $\text{Cu}^{\text{I}}$  shifts MLCT excited states to higher energies and usually leads to situations, in which ligand-based (or other) states are energetically lower and therefore dominate the photophysical and photochemical properties.<sup>34</sup>

Moreover,  $\text{Zn}^{\text{II}}$  complexes have a tendency to form polynuclear compounds,<sup>35,36</sup> many of which are labile and for which proper characterization and speciation in solution are not trivial because multiple species can exist in dynamic equilibrium with each other.<sup>37,38</sup> Thus, the lack of ligand field stabilization energy in the  $3d^{10}$  valence electron configuration can make it more challenging to obtain easily characterizable and substitution-inert mononuclear complexes compared to the above-mentioned  $3d^6$  or  $3d^8$  configurations.

The most frequently observed emission type in  $\text{Zn}^{\text{II}}$  complexes until now is ligand-based fluorescence, for example, in many dipyrin-based compounds,<sup>39–45</sup> complexes with benzothiazole ligands,<sup>46–48</sup> as well as with other nitrogen and oxygen donor ligands,<sup>49,50</sup> or phosphines.<sup>51</sup> Possible applications of fluorescent  $\text{Zn}^{\text{II}}$  compounds in electro-

Received: August 10, 2022

Revised: September 22, 2022

Accepted: September 22, 2022

Published: October 11, 2022



luminescence,<sup>46,52–54</sup> including organic light-emitting diodes (OLEDs),<sup>55–57</sup> circularly polarized luminescence,<sup>58</sup> sensing,<sup>59</sup> or cell imaging, have attracted interest.<sup>60</sup> Similarly, aggregation-induced emission<sup>61–65</sup> as well as thermally activated delayed fluorescence (TADF) received substantial attention with Zn<sup>II</sup> complexes.<sup>66–69</sup>

One of the most recent fundamental developments concerning photoactive Zn<sup>II</sup> compounds pursues the idea to introduce other emission types than ligand-based fluorescence, for example, states with triplet and/or charge-transfer character in halide complexes.<sup>70–72</sup> To date, this specific research thrust seems to concentrate largely on the solid state, presumably because phosphorescence and charge-transfer emission are trickier to obtain in fluid solution at room temperature. The solution phase is however very relevant for photoactive triplet and charge-transfer excited states, due to possible applications in triplet energy-transfer catalysis,<sup>73</sup> triplet–triplet annihilation upconversion,<sup>74</sup> photoinduced electron transfer, and photo-redox catalysis,<sup>75</sup> including perspectives for solar energy conversion.<sup>76</sup> In the course of our research program on photoactive complexes based on abundant transition metals,<sup>28,77</sup> we therefore aimed to explore the possibility of obtaining Zn<sup>II</sup> compounds with triplet charge-transfer excited states and furthermore wished to assess their potential for usage in energy-transfer catalysis, upconversion, and photo-induced electron transfer.

Our molecular design was inspired by an earlier study of Zn<sup>II</sup>-based TADF emitters with (2-hydroxyphenyl)benzoxazole ligands,<sup>66</sup> to which we attached di(anisyl)amino substituents in an attempt to enhance the charge-transfer character between the electron-rich phenolate ligand moiety and the electron-deficient benzoxazole subunit (Figure 1). We anticipated that

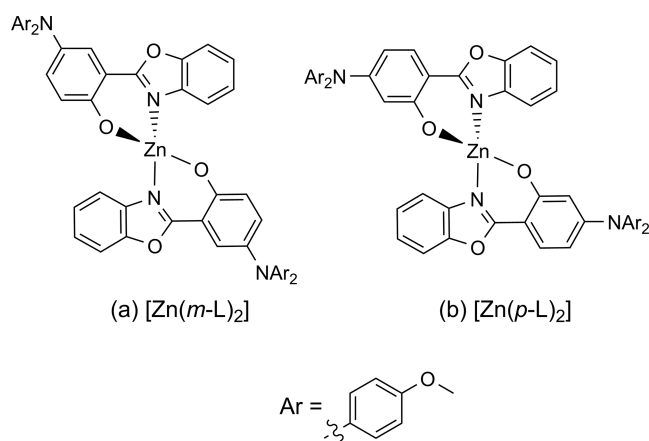


**Figure 1.** Molecular structures of the two complexes synthesized and investigated herein. Only one of two possible stereoisomers is displayed for each complex (the individual enantiomers are shown schematically in Figure S1).

this design introduces photoactive intraligand charge-transfer (ILCT) excited states and that the metal center will contribute to mediating intersystem crossing. The anticipated <sup>3</sup>ILCT excited state was further expected to be less distorted than the MLCT excited state of four-coordinate Cu<sup>I</sup> complexes, in which Jahn–Teller distortions leading to nonradiative deactivation can typically occur.<sup>3,17,78,79</sup>

## RESULTS AND DISCUSSION

### Synthesis and Characterization

Two new ligands with di(anisyl)amino substituents either in *meta*- (*m*-LH) or in *para*-position (*p*-LH) to the benzoxazole unit were synthesized and fully characterized, as described in detail in the Supporting Information (SI, pages S3–S14). The electronic coupling between the tertiary amine donor and the benzoxazole acceptor subunits is expected to be different in *m*-LH and *p*-LH, which in turn should lead to distinct properties of the anticipated ILCT excited states in [Zn(*m*-L)<sub>2</sub>] and [Zn(*p*-L)<sub>2</sub>]. Complexation was achieved by refluxing two equivalents of *m*-LH or *p*-LH with Zn(OAc)<sub>2</sub> in tetrahydrofuran (THF) or toluene overnight, following a previously published protocol for somewhat related Zn<sup>II</sup> compounds.<sup>66</sup> In our case, this led to products with ill-defined <sup>1</sup>H-NMR spectra, and MALDI-TOF-MS furthermore indicated the formation of dinuclear [Zn<sub>2</sub>(*m*-L)<sub>3</sub>] or [Zn<sub>2</sub>(*p*-L)<sub>3</sub>] complexes with *m/z* = 1443, in addition to the anticipated signals for [Zn(*m*-L)<sub>2</sub>] or [Zn(*p*-L)<sub>2</sub>] at *m/z* = 938. Evidently, product mixtures were present, and therefore the yellow powders were heated to 220 °C in a sublimation apparatus under vacuum overnight, which resulted in the deposition of free *m*-LH or *p*-LH ligand on the cooling finger. The remaining powders in the sublimation flask gave well-defined NMR signals for pure [Zn(*m*-L)<sub>2</sub>] and [Zn(*p*-L)<sub>2</sub>], and the MALDI-TOF-MS signals for the dinuclear [Zn<sub>2</sub>(*m*-L)<sub>3</sub>] or [Zn<sub>2</sub>(*p*-L)<sub>3</sub>] complexes were no longer present. The identity and purity of the mononuclear target complexes were furthermore confirmed by elemental analysis and HR-ESI-MS.

### Photophysical Properties

The UV–vis absorption spectra of [Zn(*m*-L)<sub>2</sub>] and [Zn(*p*-L)<sub>2</sub>] in toluene and dichloromethane (solid blue and black traces in Figure 2) are very similar to the spectra of the respective free

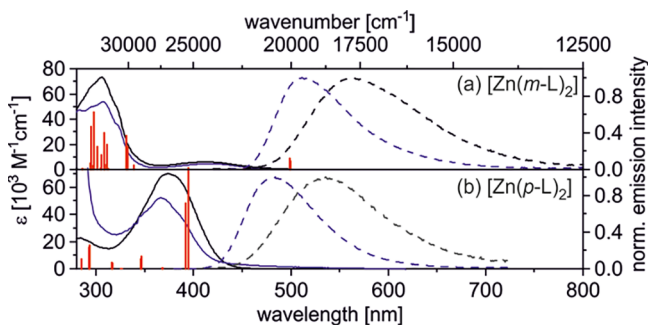


**Figure 2.** UV–vis absorption (solid lines) and normalized emission spectra (dashed lines) of (a) [Zn(*m*-L)<sub>2</sub>] (excited at 419 nm) and (b) [Zn(*p*-L)<sub>2</sub>] (excited at 370 nm) in deaerated toluene (blue) and deaerated CH<sub>2</sub>Cl<sub>2</sub> (black) at 293 K. The relative oscillator strengths of the first 60 vertical transitions (S<sub>1</sub>–S<sub>60</sub>) were calculated by TD-DFT. Vertical transitions with energy below 4.43 eV (corresponding to 280 nm) are displayed as red vertical lines.

ligands measured under identical conditions (Figures S2 and S3). Wavelength differences of absorption band maxima between complexes and respective free ligands are minimal, but the molar extinction coefficients are roughly twice as high for the complexes, due to the presence of two ligands per complex.

Strong emission solvatochromism is observed for both the complexes and the free ligands, manifesting in a redshift of

about  $2000\text{ cm}^{-1}$  when going from toluene to  $\text{CH}_2\text{Cl}_2$ . This observation suggests that the electronic transition responsible for the emission has substantial charge-transfer character, as expected. When comparing the absorption and emission properties of the two complexes, the key differences are that  $[\text{Zn}(m\text{-L})_2]$  has a distinct and comparatively weak absorption band in the visible region (with  $\epsilon = 4550\text{ M}^{-1}\text{ cm}^{-1}$  at the maximum at 417 nm in toluene), while the lowest absorption band maximum of  $[\text{Zn}(p\text{-L})_2]$  is in the UV (366 nm in toluene) and features a substantially higher molar extinction coefficient at this wavelength ( $\epsilon = 52,000\text{ M}^{-1}\text{ cm}^{-1}$ ). The emission band maximum of  $[\text{Zn}(m\text{-L})_2]$  is red-shifted compared to  $[\text{Zn}(p\text{-L})_2]$  (28 nm in toluene and 27 nm in  $\text{CH}_2\text{Cl}_2$ ). DFT calculations (SI, pages S55–S66) reproduce the experimentally observable main differences in UV–vis absorption spectroscopy. Specifically, distinct transitions at wavelengths longer than 400 nm for  $[\text{Zn}(m\text{-L})_2]$  are obtained (red vertical lines in Figure 2a), whereas for  $[\text{Zn}(p\text{-L})_2]$ , no such long-wavelength absorption transitions are calculated (red vertical lines in Figure 2b).

The DFT calculations furthermore confirm the anticipated intraligand charge-transfer (ILCT) character of the lowest-energy transitions in the two  $\text{Zn}^{\text{II}}$  complexes (Figure 3).

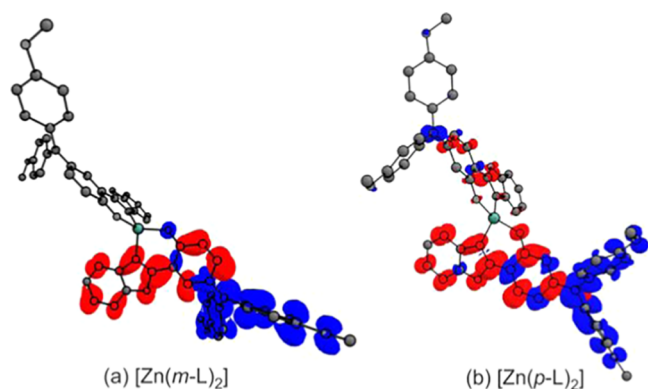


**Figure 3.** Highest occupied natural transition orbital (HONTO, blue) and lowest unoccupied natural transition orbital (LUNTO, red) of the first vertical transition ( $S_0 \rightarrow S_1$ ) of (a)  $[\text{Zn}(m\text{-L})_2]$  and (b)  $[\text{Zn}(p\text{-L})_2]$ . The  $\text{Zn}^{\text{II}}$  cation is colored in green.

Specifically, the  $S_0 \rightarrow S_1$  transition of both complexes involves a depletion of electron density from the tertiary amine units (marked blue in Figure 3) and a corresponding increase in the phenoxazole moieties (colored in red), with very little metal involvement in both cases. In  $[\text{Zn}(m\text{-L})_2]$ , the HOMO is almost exclusively located on the bis(4-methoxyphenyl)amine units (Figures 3a and S44), whereas in  $[\text{Zn}(p\text{-L})_2]$ , the HOMO is partly distributed over the 2-phenylbenzoxazole unit (Figure 3b, S45, and S46). The LUMOs of both complexes are distributed over the remaining ligand backbone without the bis(4-methoxyphenyl)amine. Based on the experimental UV–vis absorption and emission spectra, the  $^1\text{ILCT}$  energies are 2.65 eV (467 nm) for  $[\text{Zn}(m\text{-L})_2]$  and 2.89 eV (429 nm) for  $[\text{Zn}(p\text{-L})_2]$ , whereas the calculations yield 2.46 eV for  $[\text{Zn}(m\text{-L})_2]$  and 3.19 eV for  $[\text{Zn}(p\text{-L})_2]$ . The experimental values for the  $^1\text{ILCT}$  energies were estimated by normalizing the lowest-energy absorption bands and the emission bands of the  $[\text{Zn}(m\text{-L})_2]$  and  $[\text{Zn}(p\text{-L})_2]$  complexes, and by determining the intersection of the corresponding absorption and emission bands (Figure S4). Attempts to determine the respective

$^3\text{ILCT}$  energies by recording 77 K emission spectra for  $[\text{Zn}(m\text{-L})_2]$  and  $[\text{Zn}(p\text{-L})_2]$  were unsuccessful because no phosphorescence was detectable. Instead, the 77 K emission spectra resembled those recorded at room temperature, indicating that the  $^1\text{ILCT}$  remains the only emissive excited state even at 77 K. Consequently, the  $^3\text{ILCT}$  energies were estimated from the TD-DFT calculations, and the energy-level scheme in Figure 4 is therefore entirely based on calculated state energies for internal consistency reasons.

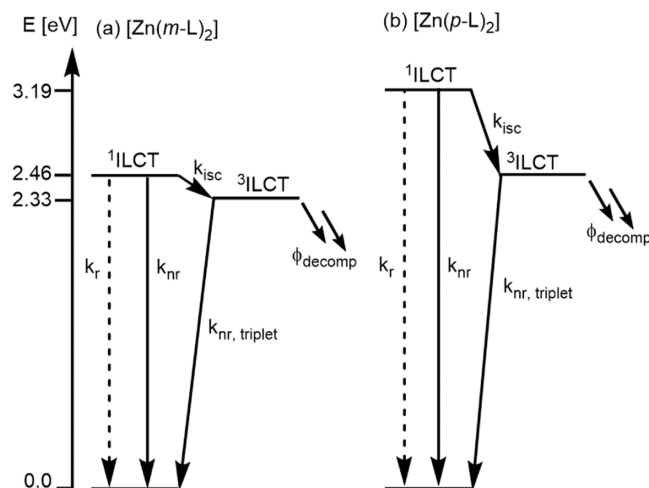


**Figure 4.** Energy-level diagrams with relative energies of the energetically lowest  $^1\text{ILCT}$  and  $^3\text{ILCT}$  excited states of  $[\text{Zn}(m\text{-L})_2]$  and  $[\text{Zn}(p\text{-L})_2]$ , as calculated by TD-DFT (PBE1PBE/def2SV(P), PCM( $\text{CH}_2\text{Cl}_2$ ); for details, see SI page S55). The lowest  $^1\text{ILCT}$  state of  $[\text{Zn}(m\text{-L})_2]$  and the lowest  $^3\text{ILCT}$  state of  $[\text{Zn}(p\text{-L})_2]$  coincidentally have the same energy (2.46 eV). Rate constants ( $k$ ) for radiative ( $r$ ) and nonradiative ( $nr$ ) relaxation processes as well as intersystem crossing ( $isc$ ) were determined experimentally and are summarized in Table 1.  $\Phi_{decomp}$  represents the quantum yield for a chemical decomposition process.

The calculated energy difference between the lowest  $^1\text{ILCT}$  and  $^3\text{ILCT}$  excited states ( $\Delta E_{ST}$ ) is substantially smaller for  $[\text{Zn}(m\text{-L})_2]$  (0.13 eV) than for  $[\text{Zn}(p\text{-L})_2]$  (0.73 eV). This can be qualitatively rationalized on the basis of the clearer spatial separation between HOMO and LUMO in  $[\text{Zn}(m\text{-L})_2]$  in comparison to  $[\text{Zn}(p\text{-L})_2]$  (due to decreased electron–electron interaction), as discussed above (Figure 3).

The UV–vis transient absorption spectra recorded at short delay times ( $<20\text{ ns}$ ) after the excitation pulses are dominated by negative signals centered around 500 nm (Figure 5), which coincide with the fluorescence bands in Figure 2. On longer time scales (microseconds), the transient absorption spectrum of  $[\text{Zn}(m\text{-L})_2]$  in deaerated toluene (Figure 5a) is dominated by an excited state absorption (ESA) band at 350 nm and a somewhat weaker ESA band centered around 610 nm. The transient difference absorption spectrum of  $[\text{Zn}(p\text{-L})_2]$  at long delay times ( $>20\text{ ns}$ ) shows a very broad ESA band with a maximum at 450 nm along with a ground-state bleach at 390 nm. Evidently,  $[\text{Zn}(m\text{-L})_2]$  and  $[\text{Zn}(p\text{-L})_2]$  both have a fluorescent singlet excited state ( $^1\text{ILCT}$ ) and a much longer-lived (nonemissive) triplet excited state ( $^3\text{ILCT}$ ), which causes the above-mentioned ESA bands. In aerated solutions of  $[\text{Zn}(m\text{-L})_2]$  and  $[\text{Zn}(p\text{-L})_2]$ , the  $^3\text{ILCT}$  excited states are efficiently quenched by oxygen (Figures 5 and S6), in line with their triplet character. Based on time-resolved fluorescence



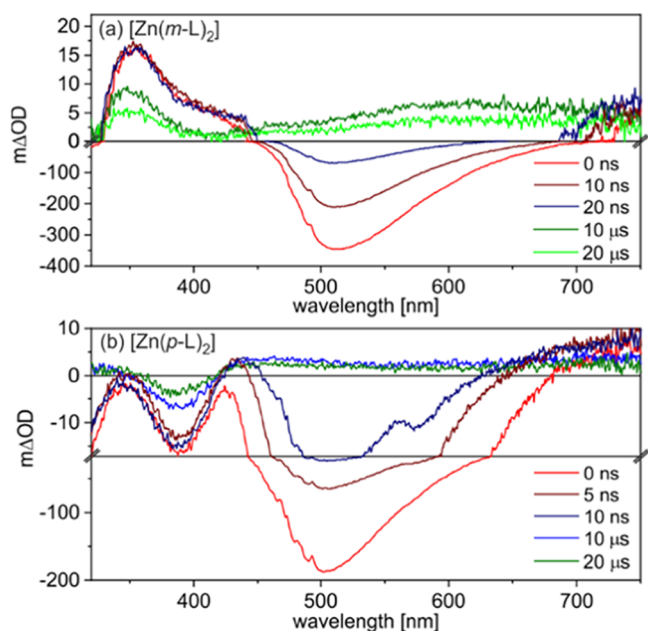


**Figure 5.** Transient absorption spectra of (a)  $[\text{Zn}(\text{m-L})_2]$  and (b)  $[\text{Zn}(\text{p-L})_2]$  in deaerated toluene at 293 K, recorded at different time delays as indicated by the legends.  $[\text{Zn}(\text{m-L})_2]$  was excited at 424 nm with laser pulse energies of 11 mJ, whereas  $[\text{Zn}(\text{p-L})_2]$  was excited at 355 nm using laser pulses with 35 mJ energy. Note the scale changes at  $\text{m}\Delta\text{OD} = 0$  in (a) and at  $\text{m}\Delta\text{OD} = -17$  in (b). All spectra were recorded with an integration time of 200 ns after the indicated delay times.

experiments (Figures S7b and S8b), the  $^1\text{ILCT}$  lifetimes ( $\tau_{\text{singlet}}$ ) of  $[\text{Zn}(\text{m-L})_2]$  and  $[\text{Zn}(\text{p-L})_2]$  are 25 and 5.5 ns, respectively, in deaerated toluene at 293 K. The  $^1\text{ILCT}$  fluorescence decay of  $[\text{Zn}(\text{m-L})_2]$  is biexponential in both toluene and  $\text{CH}_2\text{Cl}_2$ ; see SI page S23 for details. We speculate that the biexponential nature of the excited-state decay for this compound stems from different conformers that are present in solution. The  $\tau_{\text{singlet}}$  values reported for  $[\text{Zn}(\text{m-L})_2]$  in Table 1 therefore represents a weighted average (SI page S23).

Expectedly, the fluorescence lifetimes of the free ligands and corresponding complexes are very similar to each other. In toluene, the  $^1\text{ILCT}$  lifetime of  $[\text{Zn}(\text{m-L})_2]$  is longer (25 ns) than in  $\text{CH}_2\text{Cl}_2$  (9 ns), in line with the energy gap law, though for  $[\text{Zn}(\text{p-L})_2]$  such a difference is not observed and the  $^1\text{ILCT}$  lifetime is 5.5 ns in both solvents (Table S3). The fluorescence quantum yield ( $\Phi_{\text{fluor}}$ ) of  $[\text{Zn}(\text{p-L})_2]$  (86% in deaerated toluene at 293 K, Table 1) is substantially higher than that of  $[\text{Zn}(\text{m-L})_2]$  under identical conditions (50%). With  $^1\text{ILCT}$  lifetimes and luminescence quantum yields at hand, the rate constants for radiative ( $k_r$ ) and nonradiative excited-state relaxation ( $k_{\text{nr}}$ ) were calculated following eqs S5–S9. The

intense fluorescence signals and rapid intersystem crossing complicate the detection of the spectral signatures of the  $^1\text{ILCT}$  states by transient absorption, but it seems plausible that the  $^1\text{ILCT}$  and  $^3\text{ILCT}$  states have in fact similar spectroscopic signatures (Figures 5 and S6).<sup>80</sup> Based on their very different decay kinetics, the distinction between these two states is however clear-cut.

To obtain quantitative information concerning the inter-system crossing (ISC) from the initially excited  $^1\text{ILCT}$  to the (dark)  $^3\text{ILCT}$  state, relative actinometry experiments were performed. For this purpose, the molar quantities of triplet-excited anthracene formed after selective excitation of  $[\text{Zn}(\text{m-L})_2]$  and  $[\text{Zn}(\text{p-L})_2]$  in the presence of excess anthracene were determined by transient UV–vis absorption spectroscopy (Figure 6). Assuming that triplet–triplet energy transfer from the  $\text{Zn}^{\text{II}}$  complexes to anthracene is quantitative (which seems reasonable given its high driving force) and given the known molar extinction coefficient of triplet-excited anthracene at 423 nm ( $53,000 \text{ M}^{-1} \text{ cm}^{-1}$ ),<sup>81</sup> the concentration of triplet-excited  $[\text{Zn}(\text{m-L})_2]$  and  $[\text{Zn}(\text{p-L})_2]$  can be estimated in this manner. In a separate experiment, an aqueous solution of  $[\text{Ru}(\text{bpy})_3]^{2+}$  with the same absorbance at the respective excitation wavelength was irradiated using identical instrument settings. By monitoring the bleach of the corresponding MLCT absorption band at 455 nm with its known change in molar extinction coefficient ( $\Delta\epsilon = -10,100 \text{ M}^{-1} \text{ cm}^{-1}$ ),<sup>82</sup> the number of photons absorbed by the individual solutions was determined; see SI page S20 for full details. The intersystem crossing quantum yield ( $\Phi_{\text{isc}}$ ) was then approximated as the number of triplet-excited  $\text{Zn}^{\text{II}}$  complexes divided by the number of absorbed photons.

For  $[\text{Zn}(\text{m-L})_2]$ , we obtain  $\Phi_{\text{isc}} = 13\%$ , whereas for  $[\text{Zn}(\text{p-L})_2]$ ,  $\Phi_{\text{isc}}$  is substantially lower with merely 7.2%. This finding is compatible with the lower fluorescence quantum yield found for  $[\text{Zn}(\text{m-L})_2]$  (50%) relative to  $[\text{Zn}(\text{p-L})_2]$  (86%), and furthermore is in qualitative accordance with the smaller  $^1\text{ILCT}$ – $^3\text{ILCT}$  energy gap ( $\Delta E_{\text{ST}}$ ) in  $[\text{Zn}(\text{m-L})_2]$  (0.13 vs 0.73 eV, Figure 4), as  $k_{\text{isc}}$  is often inversely proportional to  $\Delta E_{\text{ST}}$ .<sup>83</sup>

By monitoring the decay of the excited-state absorption band at 350 nm in Figure 5a (Figure S9) and the bleach recovery at 390 nm in Figure 5b (Figure S10), the lifetimes of the photoactive (but dark)  $^3\text{ILCT}$  excited states ( $\tau_{\text{triplet}}$ ) of  $[\text{Zn}(\text{m-L})_2]$  and of  $[\text{Zn}(\text{p-L})_2]$  were determined. We find  $\tau_{\text{triplet}} = 38 \mu\text{s}$  for  $[\text{Zn}(\text{m-L})_2]$  and  $\tau_{\text{triplet}} = 62 \mu\text{s}$  for  $[\text{Zn}(\text{p-L})_2]$  in deaerated toluene at 293 K.

### Triplet Energy-Transfer Catalysis

Since both  $[\text{Zn}(\text{m-L})_2]$  and  $[\text{Zn}(\text{p-L})_2]$  have appreciable intersystem crossing quantum efficiencies (Table 1 and Figure 6), we decided to explore to what extent these compounds can sensitize organic triplet excited-state reactions, such as photo-isomerizations and a photo-fragmentation. We used a 415 nm

**Table 1.** Experimental Values of  $^1\text{ILCT}$  ( $\tau_{\text{singlet}}$ ) and  $^3\text{ILCT}$  Lifetimes ( $\tau_{\text{triplet}}$ ), Fluorescence and Intersystem Crossing Quantum Yields ( $\Phi_{\text{fluor}}$  and  $\Phi_{\text{isc}}$ ) in Deaerated Toluene at 293 K<sup>ab</sup>

	$\tau_{\text{singlet}}$ [ns]	$\tau_{\text{triplet}}$ [ $\mu\text{s}$ ]	$\Phi_{\text{fluor}}$ [%]	$\Phi_{\text{isc}}$ [%]	$k_{\text{tot}}$ [ $\text{s}^{-1}$ ]	$k_r$ [ $\text{s}^{-1}$ ]	$k_{\text{nr}}$ [ $\text{s}^{-1}$ ]	$k_{\text{isc}}$ [ $\text{s}^{-1}$ ]	$k_{\text{nr,triplet}}$ [ $\text{s}^{-1}$ ]
m-LH	24		22		$4.2 \times 10^7$	$9.2 \times 10^6$	$3.3 \times 10^7$		
$[\text{Zn}(\text{m-L})_2]$	25 <sup>b</sup>	38	50	13	$4.0 \times 10^7$	$2.0 \times 10^7$	$1.5 \times 10^7$	$5.2 \times 10^6$	$2.6 \times 10^4$
p-LH	5.5		94		$1.8 \times 10^8$	$1.7 \times 10^8$	$1.0 \times 10^7$		
$[\text{Zn}(\text{p-L})_2]$	5.5	62	86	7.2	$1.8 \times 10^8$	$1.5 \times 10^8$	$1.2 \times 10^7$	$1.3 \times 10^7$	$1.6 \times 10^4$

<sup>a</sup>The radiative ( $k_r$ ) and nonradiative rate constants ( $k_{\text{nr}}$ ) for  $^1\text{ILCT}$  decay, as well as the rate constant for nonradiative  $^3\text{ILCT}$  decay ( $k_{\text{nr,triplet}}$ ) as illustrated in Figure 4 are as indicated. <sup>b</sup>Lifetimes of biexponential decays were averaged in a weighted manner (see SI page S22 for details).

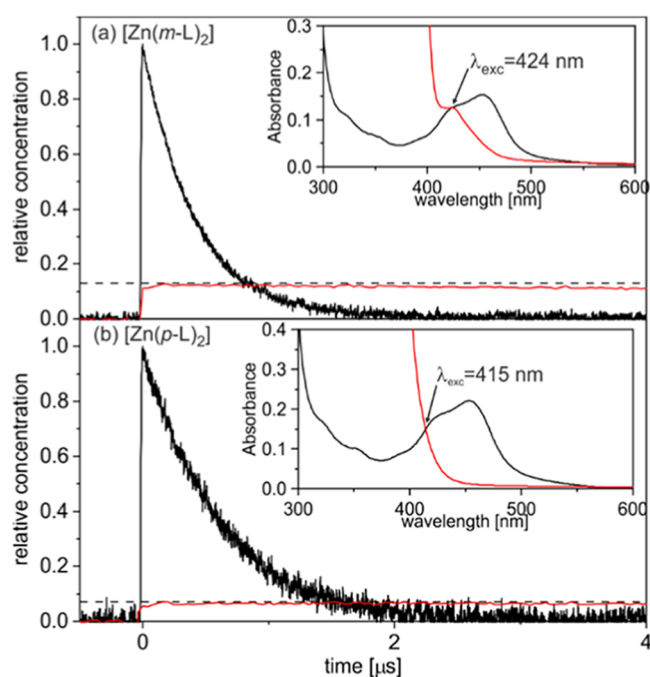


**Figure 6.** Determination of the intersystem crossing quantum yield ( $\Phi_{\text{isc}}$ ) by monitoring the formation of triplet-excited anthracene following excitation of  $[\text{Zn}(\text{m-L})_2]$  and  $[\text{Zn}(\text{p-L})_2]$  in the presence of 10 mM anthracene. Solutions of  $[\text{Ru}(\text{bpy})_3]^{2+}$  in deaerated  $\text{H}_2\text{O}$  at 293 K with identical absorbance at the excitation wavelengths ( $\lambda_{\text{exc}} = 424/415$  nm, insets) were used to determine the number of photons absorbed by the individual solutions. The black trace in both main plots is the  $^3\text{MLCT}$  excited state decay of  $[\text{Ru}(\text{bpy})_3]^{2+}$  monitored at 455 nm, where  $\Delta\epsilon = -10,100 \text{ M}^{-1} \text{ cm}^{-1}$  upon  $^3\text{MLCT}$  excitation.<sup>82</sup> The red traces in both main plots represent the relative amounts of triplet-excited anthracene following excitation of (a) 27  $\mu\text{M}$   $[\text{Zn}(\text{m-L})_2]$  at 424 nm and (b) 8.5  $\mu\text{M}$   $[\text{Zn}(\text{p-L})_2]$  at 415 nm in deaerated toluene at 293 K, both in the presence of 10 mM anthracene (determined by monitoring the diagnostic triplet anthracene absorption band at 423 nm with  $\epsilon = 53,000 \text{ M}^{-1} \text{ cm}^{-1}$ ).<sup>81</sup> Assuming that triplet–triplet energy transfer from the  $^3\text{ILCT}$  excited state of the  $\text{Zn}^{\text{II}}$  complexes is quantitative under these conditions, the intersystem crossing quantum yields can be estimated from the transient absorption signals at  $t = 0$  (red vs black decay traces). The insets show UV–vis (ground state) absorption spectra of all used solutions, demonstrating that  $[\text{Ru}(\text{bpy})_3]^{2+}$  (black) and the solutions of the  $\text{Zn}^{\text{II}}$  complexes absorbed equal amounts of light at the used excitation wavelengths ( $\lambda_{\text{exc}}$ ).

LED as an excitation source for these purposes. For the first experiment, we adjusted the  $[\text{Zn}(\text{m-L})_2]$  and  $[\text{Zn}(\text{p-L})_2]$  concentrations such that an optical density of 0.06 resulted at that wavelength, which implied substantially different complex concentrations (1.3 vs 0.6 mol % relative to the substrates) due to their different molar extinction coefficients at 415 nm (Figure 2). This procedure was chosen to ensure that the different reaction mixtures absorb equal amounts of excitation light in a given irradiation period.

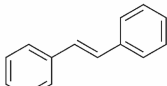
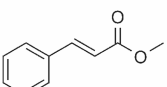
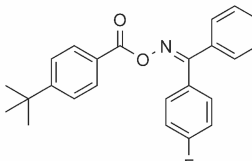
Under these conditions, the photo-isomerization of *trans*-stilbene reached the photostationary state after about 60 min (Figure S22). With  $[\text{Zn}(\text{m-L})_2]$  as photosensitizer, that photostationary state was composed of 81% *cis*-stilbene, whereas the  $[\text{Zn}(\text{p-L})_2]$  complex yielded a photostationary state with only 49% of *cis*-stilbene (Table 2, entry 1). This experimental observation can be understood on the basis of the different triplet energies of the two photosensitizers (Figure 4)

and the different triplet energies of *trans*-stilbene (2.14 eV) and *cis*-stilbene (2.35 eV) (Figure S18).<sup>84</sup> The  $^3\text{ILCT}$  energy of  $[\text{Zn}(\text{m-L})_2]$  (2.33 eV) lies between the triplet energies of *trans*- and *cis*-stilbene, and consequently this complex sensitizes the *trans*-to-*cis* photo-isomerization of stilbene far more efficiently than the reverse reaction, resulting in the accumulation of the *cis*-isomer over time (Table 2, entry 1). By contrast, the photoactive  $^3\text{ILCT}$  state of  $[\text{Zn}(\text{p-L})_2]$  (2.46 eV) is energetically above the lowest triplet states of both *trans*- and *cis*-stilbene. Consequently,  $[\text{Zn}(\text{p-L})_2]$  sensitizes the *cis*-to-*trans* and the *trans*-to-*cis* photo-isomerization of this specific substrate equally well, resulting in a photostationary state composed of roughly 1:1 *cis*- and *trans*-products (Table 2, entry 1, last column). Though photo-isomerizations of stilbene compounds have been reported after direct excitation of their singlet excited states,<sup>85–87</sup> we have found no evidence that the fluorescent  $^1\text{ILCT}$  excited states of our zinc(II) complexes sensitize this reaction.

For the methyl cinnamate substrate (Table 2, entry 2), the  $[\text{Zn}(\text{m-L})_2]$  photosensitizer leads to a photostationary state containing only 30% of the *cis*-isomer, which is considerably lower than what is obtained in the case of stilbene (81%). This observation can be understood on the basis of the higher triplet energy of *trans*-methyl cinnamate (2.37 eV)<sup>84</sup> compared to *trans*-stilbene (2.14 eV).<sup>84</sup> Consequently,  $[\text{Zn}(\text{m-L})_2]$  with its  $^3\text{ILCT}$  energy of 2.33 eV becomes a less efficient sensitizer for the *cis*-to-*trans* isomerization of methyl cinnamate. When using  $[\text{Zn}(\text{p-L})_2]$  as a sensitizer for the methyl cinnamate substrate, a substantially higher *cis* photoproduct yield of 49% is reached, due to the higher  $^3\text{ILCT}$  energy of this complex in comparison to  $[\text{Zn}(\text{m-L})_2]$ . For the methyl cinnamate photo-isomerization reactions, we used an identical photosensitizer loading of 0.5 mol % in both experiments. When reducing the catalyst load to 0.05 mol %, we determined a turnover number (TON) of 550 for  $[\text{Zn}(\text{m-L})_2]$  and 940 for  $[\text{Zn}(\text{p-L})_2]$ .

To explore organic triplet reactivity beyond photo-isomerizations, we focused on a decarboxylation reaction (Table 2, entry 3), which was previously sensitized by an iridium complex with a triplet energy of 2.64 eV.<sup>88</sup> Following excitation to its lowest-lying triplet state, this substrate is known to undergo a photo-fragmentation reaction that is triggered by the release of  $\text{CO}_2$ , forming an aryl radical intermediate. The latter can be intercepted by  $\text{CDCl}_3$  under uptake of a deuterium atom, which makes the respective fragmentation product (Table 2, entry 3) easily detectable by NMR spectroscopy. Unfortunately, in  $\text{CDCl}_3$  the solubility of  $[\text{Zn}(\text{m-L})_2]$  and  $[\text{Zn}(\text{p-L})_2]$  is limited and furthermore both complexes suffer from lower stability in  $\text{CDCl}_3$  compared to less polar solvents such as benzene or toluene. Conversely, the substrate is not sufficiently well soluble in benzene- $d_6$  and toluene- $d_8$ . Consequently, only relatively modest decarboxylation yields of 8% when using  $[\text{Zn}(\text{m-L})_2]$  and 18% in the case of  $[\text{Zn}(\text{p-L})_2]$  were obtained (Table 2, entry 3; Figures S27–S30). Upon irradiation of a solution of the substrate without  $\text{Zn}^{\text{II}}$  photosensitizer, no decarboxylation product can be observed (Figures S31 and S32), which confirms the triplet sensitization of the substrate by the  $[\text{Zn}(\text{m-L})_2]$  and  $[\text{Zn}(\text{p-L})_2]$  complexes. Compared to the previously used iridium complex, the  $\text{Zn}^{\text{II}}$  sensitizers employed here have substantially lower triplet energies (2.33 and 2.46 vs 2.64 eV), which might help explain the lower photo-fragmentation yields observed here.<sup>88</sup> Moreover, iminyl-radicals formed in the photo-fragmentation reaction could potentially poison the catalyst

Table 2. Sensitized Triplet–Triplet Energy-Transfer (TTET) Reactions

Entry	Reaction	Photocatalyst	
		[Zn( <i>m</i> -L) <sub>2</sub> ]	[Zn( <i>p</i> -L) <sub>2</sub> ]
1	 photocat. (0.6–1.3 mol%) <sup>a</sup> hv (415 nm, 7 W, 385 nm filter) C <sub>6</sub> D <sub>6</sub> , RT, 1.0 h	81% <sup>b</sup>	49% <sup>b</sup>
2	 photocat. (0.5 mol%) Me <sub>3</sub> SiPh (0.33 eq.) hv (415 nm, 7 W, 400 nm filter) C <sub>6</sub> D <sub>6</sub> , RT, 3.0 h	30% <sup>c</sup>	49% <sup>c</sup>
3	 photocat. (1.0 mol%) Me <sub>3</sub> SiPh (1.0 eq.) hv (415 nm, 7 W, 400 nm filter) CDCl <sub>3</sub> , RT, 3.5 h	8% <sup>c</sup>	18% <sup>c</sup>

<sup>a</sup>Optical densities adjusted to the same value of about 0.06 at the excitation wavelength of 415 nm for both complexes, resulting in 1.3 mol % [Zn(*m*-L)<sub>2</sub>] and 0.6 mol % [Zn(*p*-L)<sub>2</sub>]. <sup>b</sup>Yields were determined by comparing <sup>1</sup>H-NMR integrals of the reactant and the product. <sup>c</sup>Yields were calculated relative to the internal standard Me<sub>3</sub>SiPh using <sup>1</sup>H-NMR spectroscopy.

because the Zn<sup>II</sup> complexes are expected to be considerably more substitution-labile than cyclometalated Ir<sup>III</sup> compounds.

#### Photoinduced Electron Transfer Reactivity

Given the charge-transfer character of the photoactive excited states of [Zn(*m*-L)<sub>2</sub>] and [Zn(*p*-L)<sub>2</sub>], it seemed meaningful to explore their ability to undergo photoinduced electron transfer reactions. Toward this end, we identified 1,2,4,5-tetracyanobenzene (TCB) as a suitable reaction partner because this is a fairly strong electron acceptor featuring a reduction potential of −0.74 V vs SCE in MeCN,<sup>89</sup> combined with a characteristic spectroscopic signature of its one-electron reduced form (TCB<sup>•−</sup>), which is readily identifiable by transient UV–vis absorption spectroscopy.

After selective excitation of [Zn(*m*-L)<sub>2</sub>] at 420 nm in the presence of excess TCB, the resulting UV–vis transient absorption difference spectrum (Figure 7b) is essentially a 1:1 superposition of the spectral signatures of TCB<sup>•−</sup> (Figure 7a)<sup>90,91</sup> and [Zn(*m*-L)<sub>2</sub>]<sup>+</sup> (Figure 7c). The latter resembles very closely the typical spectral signatures of triarylammonium radical cations,<sup>92</sup> in line with the fact that the primary oxidation of [Zn(*m*-L)<sub>2</sub>] occurs on the triarylamine unit of the chelate ligand. For [Zn(*m*-L)<sub>2</sub>]<sup>+</sup> the respective absorption band is observed near 750 nm (Figure 7b), whereas for [Zn(*p*-L)<sub>2</sub>]<sup>+</sup>, the analogous absorption band is shifted to near 800 nm (Figure S36c).

In time-correlated single photon counting (TCSPC) experiments, no significant quenching of the <sup>1</sup>ILCT fluorescence of [Zn(*m*-L)<sub>2</sub>] and [Zn(*p*-L)<sub>2</sub>] by 2.5 mM TCB was observed, suggesting that photoinduced electron transfer to TCB occurs from the long-lived <sup>3</sup>ILCT states of the Zn<sup>II</sup> complexes, not from the fluorescent <sup>1</sup>ILCT states. Indeed, in laser flash photolysis experiments, quenching of the <sup>3</sup>ILCT states of [Zn(*m*-L)<sub>2</sub>] and [Zn(*p*-L)<sub>2</sub>] by TCB is detectable by monitoring the characteristic absorption bands and ground-state bleaches of the <sup>3</sup>ILCT excited Zn<sup>II</sup> complexes at 350 and 390 nm (Figure 5), respectively. By monitoring the <sup>3</sup>ILCT decays as a function of the TCB concentration (Figures S34 and S35), the Stern–Volmer-type plots in the insets of Figures 7b and S33b were obtained. Linear regression fits to these data

gave rate constants of  $5.3 \times 10^9$  and  $6.3 \times 10^9$  M<sup>−1</sup> s<sup>−1</sup> for photoinduced electron transfer from [Zn(*m*-L)<sub>2</sub>] and [Zn(*p*-L)<sub>2</sub>] to TCB, respectively. These values are relatively close to the diffusion limit in toluene at 293 K ( $1.1 \times 10^{10}$  M<sup>−1</sup> s<sup>−1</sup>),<sup>84</sup> in line with a high driving-force reaction. In cyclic voltammetry, the first oxidation wave appears at 0.32 V vs SCE for [Zn(*m*-L)<sub>2</sub>] (Figure S13) and at 0.80 V vs SCE for [Zn(*p*-L)<sub>2</sub>] (Figure S15). Given the <sup>3</sup>ILCT energies in Table 1, we estimate excited-state oxidation potentials of −2.01 V vs SCE for [Zn(*m*-L)<sub>2</sub>] (Figure S16) and −1.66 V vs SCE for [Zn(*p*-L)<sub>2</sub>] (Figure S17). Consequently, photoinduced electron transfer to TCB (featuring a reduction potential of −0.74 V vs SCE in MeCN)<sup>89</sup> is highly exergonic in both cases, which can explain why nearly diffusion-controlled kinetics are observed.

According to this analysis, the two Zn<sup>II</sup> complexes are both rather strong photoreductants, but [Zn(*m*-L)<sub>2</sub>] is roughly 0.4 V more reducing in its <sup>3</sup>ILCT excited state than [Zn(*p*-L)<sub>2</sub>]. This finding can be traced back to substantially different ground-state oxidation potentials, which might have their origin in different extents of electronic coupling between the coordinating phenolate units and the triarylamine N-atoms. Specifically, in [Zn(*m*-L)<sub>2</sub>], the anionic phenolate unit stands in *para*-position to the triarylamine N-atom, which might enhance the electron density at the N-atom and could lower the respective oxidation potential in comparison to [Zn(*p*-L)<sub>2</sub>], in which the phenolate unit stands in *meta*-position to the triarylamine N-atom.

#### Blue to Ultraviolet Upconversion

With their photoactive <sup>3</sup>ILCT excited states, both [Zn(*m*-L)<sub>2</sub>] and [Zn(*p*-L)<sub>2</sub>] should in principle be able to sensitize triplet–triplet annihilation upconversion, which is an attractive process for the conversion of low-energy input light into higher energy output radiation.<sup>74,93–96</sup> In particular, upconversion from the visible to the ultraviolet spectral region has received increasing interest lately,<sup>97–102</sup> and our Zn<sup>II</sup> complexes with their relatively high <sup>3</sup>ILCT energies seemed promising for this purpose. Previous upconversion studies with Zn<sup>II</sup> sensitizers focused on red-to-blue upconversion and on near-infrared



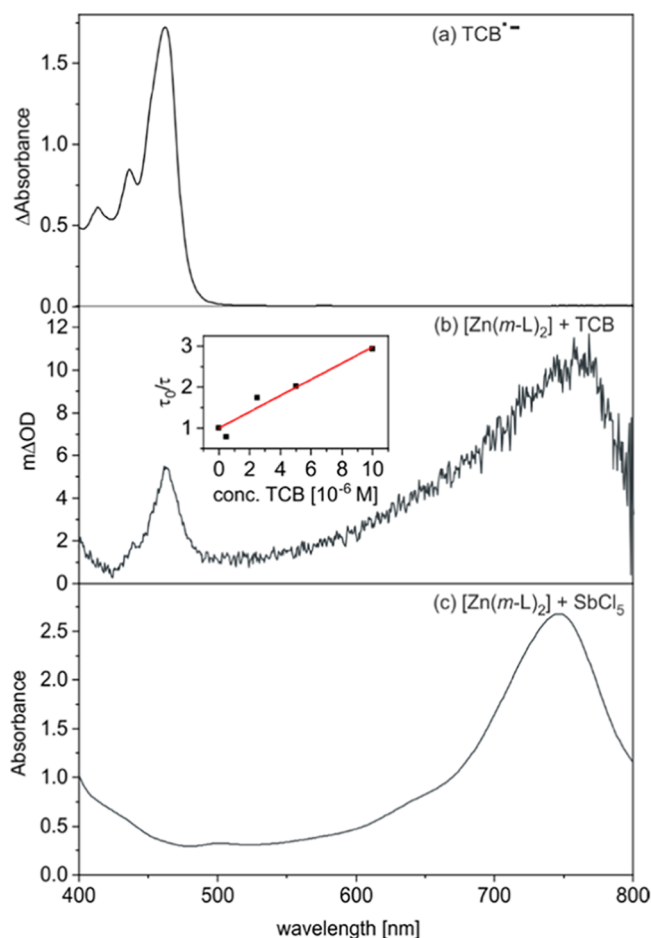


**Figure 7.** (a) UV-vis difference spectrum obtained upon electrochemical reduction of 1,2,4,5-tetracyanobenzene (TCB, 2.5 mM) in deaerated MeCN in the presence of  $N(n\text{Bu})_4\text{PF}_6$  (0.1 M) as supporting electrolyte, obtained by applying a voltage sufficient to induce one-electron reduction of TCB. (b) Transient absorption difference spectrum of 45  $\mu\text{M}$   $[\text{Zn}(m\text{-L})_2]$  and 2.5 mM TCB in deaerated toluene at 293 K, recorded 1  $\mu\text{s}$  after excitation at 420 nm with laser pulses with an energy of 12 mJ. Inset: Stern-Volmer-type plot for the oxidative excited-state quenching of  $[\text{Zn}(m\text{-L})_2]$  by TCB in deaerated toluene, obtained by monitoring an excited state absorption band at 350 nm ( $k_q = 5.3 \times 10^9 \text{ M}^{-1} \text{ s}^{-1}$ , Figure S31). (c) Absorption spectrum of  $[\text{Zn}(m\text{-L})_2]^+$  in deaerated  $\text{CH}_2\text{Cl}_2$  at 293 K, obtained after chemical oxidation of a  $[\text{Zn}(m\text{-L})_2]$  solution (140  $\mu\text{M}$ ) with  $\text{SbCl}_5$  (1 equiv).

sensitization of photochemical reactions.<sup>103–106</sup> We identified the combination of  $[\text{Zn}(m\text{-L})_2]$  and  $(\text{TMS})_2\text{napht}$  (Figure 8e) as particularly promising for blue to UV upconversion. Unsubstituted naphthalene has a triplet energy of 2.62 eV,<sup>84</sup> which is too high for both our  $\text{Zn}^{\text{II}}$  complexes (Figure 4). The substitution of polyaromatic hydrocarbon annihilators with protected acetylene units was previously found to lower the energies of the lowest triplet excited states.<sup>107,108</sup> For example, naphthalene substituted with triisopropylsilyl (TIPS) protected acetylenes in 1- and 4-positions has a triplet energy of 2.10 eV.<sup>98</sup> The  $(\text{TMS})_2\text{napht}$  compound (Figure 8e) differs from that previously investigated annihilator merely by the presence of trimethylsilyl (TMS) instead of TIPS groups, and therefore we anticipate a similar triplet energy of ca. 2.10 eV for  $(\text{TMS})_2\text{napht}$ . TTET from the <sup>3</sup>ILCT excited state of  $[\text{Zn}(m\text{-L})_2]$  to  $(\text{TMS})_2\text{napht}$  is thus expected to be exergonic by roughly 0.2 eV. This specific sensitizer-annihilator combination

furthermore seemed beneficial because  $[\text{Zn}(m\text{-L})_2]$  absorbs less than  $[\text{Zn}(p\text{-L})_2]$  in the spectral region of the  $(\text{TMS})_2\text{napht}$  fluorescence (350–400 nm, Figure S34), which should limit unwanted reabsorption phenomena. In the following, we aimed at a proof-of-principle experiment, to explore the application potential of tetrahedral  $\text{Zn}^{\text{II}}$  complexes for photochemical upconversion.

A solution containing 30  $\mu\text{M}$   $[\text{Zn}(m\text{-L})_2]$  and 2 mM  $(\text{TMS})_2\text{napht}$  in deaerated toluene was excited at 430 nm with laser pulses of roughly 10 ns duration and 16 mJ energy. At this wavelength,  $(\text{TMS})_2\text{napht}$  is essentially transparent and the light is absorbed exclusively by the  $\text{Zn}^{\text{II}}$  complex. Emission spectra were then recorded in a time-gated manner, once immediately after the excitation pulses (blue trace in Figure 8b) and once with a delay of 1  $\mu\text{s}$  (red trace in Figure 8b). The blue trace is dominated by the <sup>1</sup>ILCT emission of  $[\text{Zn}(m\text{-L})_2]$  centered around 528 nm, yet between 350 and 400 nm, a weak luminescence band (shown on an enlarged scale in the inset of Figure 8b) is furthermore detectable. That latter emission band also appears in the luminescence spectrum recorded with a time delay (red trace), while the fluorescence of  $[\text{Zn}(m\text{-L})_2]$  is absent in that case because the <sup>1</sup>ILCT excited state with its lifetime ( $\tau_{\text{singlet}}$ ) of 25 ns (Table 1) has completely decayed after 1  $\mu\text{s}$ . The UV emission in the inset of Figure 8b (blue and red traces) is in good agreement with the fluorescence spectrum of  $(\text{TMS})_2\text{napht}$  obtained after direct excitation at 350 nm (Figure S34), and consequently, these UV emissions are attributable to the delayed (upconverted) annihilator fluorescence. This delayed fluorescence decays on a microsecond timescale (100  $\mu\text{s}$  time gates were used to record the blue and red traces in Figure 8b) and as such reflects the lifetime of the photoactive triplet excited state of  $(\text{TMS})_2\text{napht}$ , which is populated by TTET from the <sup>3</sup>ILCT state of  $[\text{Zn}(m\text{-L})_2]$  (Figure 8d).

To estimate the upconversion quantum yield under the conditions of this pulsed laser study, an additional reference experiment was performed, in which we recorded the prompt <sup>1</sup>ILCT fluorescence of  $[\text{Zn}(m\text{-L})_2]$  under identical conditions, using a solution containing only the  $\text{Zn}^{\text{II}}$  sensitizer (20  $\mu\text{M}$ ) but no annihilator (black trace in Figure 8b). When normalizing the black and blue traces in Figure 8b, we were thus able to determine the integrated <sup>1</sup>ILCT emission intensity ( $I_{\text{flu}}$ ) and the integrated delayed annihilator fluorescence ( $I_{\text{UC}}$ ) by comparing the black and red traces in Figure 8b (SI page S48). Given a <sup>1</sup>ILCT fluorescence quantum yield ( $\Phi_{\text{flu}}$ ) of 50% (Table 1), this analysis yields an upconversion quantum yield ( $\phi_{\text{UC}}$ ) of 0.73% (relative to a theoretical limit of 50%,<sup>109</sup> SI page S48). Given the incomplete intersystem crossing in  $[\text{Zn}(m\text{-L})_2]$  ( $\Phi_{\text{isc}} = 13\%$ ), the modest upconversion quantum yield is unsurprising. Normalized to the amount of photo-generated triplet excited states on  $[\text{Zn}(m\text{-L})_2]$ , the upconversion quantum yield is 5.6%, which compares favorably to many previously investigated systems.

Excitation power-dependent measurements were performed using a 447 nm continuous-wave (cw) laser and yielded the series of upconversion fluorescence spectra shown in Figure 8a and the prompt <sup>1</sup>ILCT emission spectra in Figure 8c. When plotting the integrated (normalized) emission intensities as a function of relative excitation density, the expectable quadratic power dependence is obtained for the upconversion emission (inset of Figure 8a,  $x^{1.82}$ ), whereas the prompt <sup>1</sup>ILCT fluorescence shows the anticipated linear power dependence (inset of Figure 8c,  $x^{1.03}$ ).

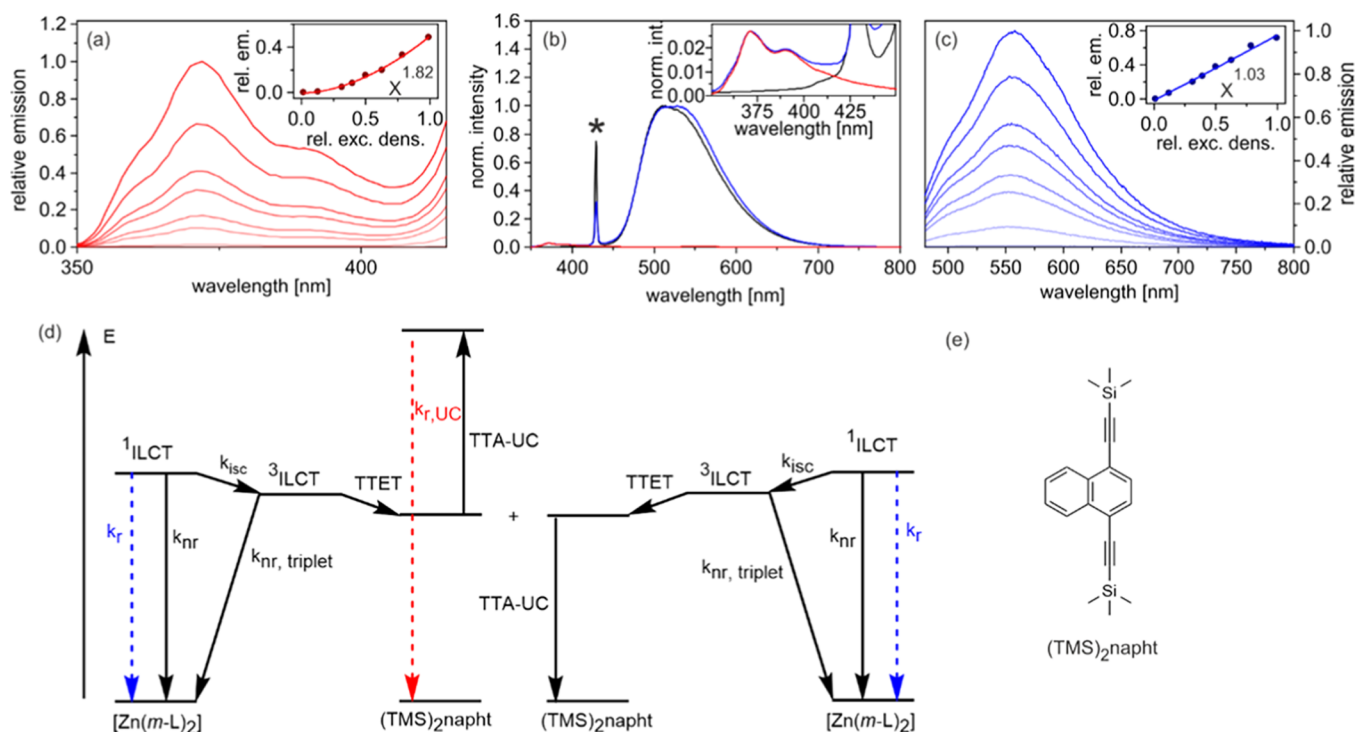


**Figure 8.** Sensitized triplet–triplet annihilation upconversion (sTTA-UC) using  $[\text{Zn}(\text{m-L})_2]$  as the sensitizer and 1,4-bis((trimethylsilyl)ethynyl)naphthalene ((TMS)<sub>2</sub>napht) as the annihilator in deaerated toluene. (a) Power dependence of the upconverted emission in a steady-state experiment with a solution containing 2 mM (TMS)<sub>2</sub>napht and 170  $\mu\text{M}$   $[\text{Zn}(\text{m-L})_2]$  excited at 447 nm. Inset: Quadratic dependence of the integrated emission intensities from the main plot of (a) on the relative excitation density. (b) Upconversion quantum yield estimation with 2 mM (TMS)<sub>2</sub>napht and 30  $\mu\text{M}$   $[\text{Zn}(\text{m-L})_2]$  under pulsed excitation at 430 nm. The blue trace is the prompt sensitizer emission (peaking at 528 nm) as well as the upconverted emission (peaking at 371 nm (seen mostly in the inset), recorded without delay, 100  $\mu\text{s}$  integration time). The red trace represents only the upconverted emission (recorded with 1  $\mu\text{s}$  delay (the prompt sensitizer emission has already decayed completely at that point), 100  $\mu\text{s}$  integration time) of the same sensitizer/annihilator solution. The black trace represents only the prompt (normalized)  $[\text{Zn}(\text{m-L})_2]$  emission (measured from a 20  $\mu\text{M}$   $[\text{Zn}(\text{m-L})_2]$  solution without annihilator, recorded without delay, 100  $\mu\text{s}$  integration time). The asterisk (\*) designates stray laser light. Inset: Upconverted emission from the main plot of (b) on an enlarged scale. (c) Power dependence of the prompt emission of  $[\text{Zn}(\text{m-L})_2]$  in a steady-state experiment with a solution containing 2 mM (TMS)<sub>2</sub>napht and 170  $\mu\text{M}$   $[\text{Zn}(\text{m-L})_2]$  excited at 447 nm. Inset: Linear dependence of the data from the main plot of (c) on the relative excitation density. (d) Energy-level diagram of the sensitizer and annihilator, along with a summary of the photophysical processes they undergo in the course of sTTA-UC. (e) Molecular structure of the annihilator 1,4-bis((trimethylsilyl)ethynyl)naphthalene ((TMS)<sub>2</sub>napht).

### Photostability of the Zn<sup>II</sup> Complexes

Many applications require long-term photo-irradiation, and thus it seemed meaningful to explore the photo-robustness of the Zn<sup>II</sup> complexes from Figure 1 in comparison with  $[\text{Ru}(\text{bpy})_3]^{2+}$ , a well-known and widely used benchmark compound.<sup>110</sup> For this purpose, deaerated solutions of  $[\text{Zn}(\text{m-L})_2]$ ,  $[\text{Zn}(\text{p-L})_2]$ , and  $[\text{Ru}(\text{bpy})_3]^{2+}$  with essentially identical absorbance values ( $A_0$ ) of 0.05 at 405 nm were prepared (Table S4) and then irradiated at that wavelength with a cw laser providing 0.526 W of output power. Following a previously published method (SI pages S43 and S44),<sup>102,111,112</sup> we monitored the emission intensity of these three complexes as a function of irradiation time and estimated their photodegradation quantum yields ( $\Phi_{\text{decomp}}$ ) by considering the time period during which their photoluminescence intensities decreased to 90% of the initial values at  $t = 0$  (SI page S43). Given the known (initial) concentrations of the complexes ( $c_0$ ) and the measurable number of photons absorbed within the above-mentioned time period (the initial absorbance values  $A_0$  are known, and the laser power is known as well), the  $\Phi_{\text{decomp}}$  values in Table 3 were obtained (Table S4). In comparison to  $[\text{Ru}(\text{bpy})_3]^{2+}$ , the inherent photostability of the two investigated Zn<sup>II</sup> complexes is an order of

**Table 3. Photodegradation Quantum Yields ( $\Phi_{\text{decomp}}$ ) of  $[\text{Zn}(\text{m-L})_2]$ ,  $[\text{Zn}(\text{p-L})_2]$ , and  $[\text{Ru}(\text{bpy})_3]^{2+}$  in Deaerated Solutions at 293 K Irradiated with a 405 nm cw Laser (Power Output of 0.526 W)**

complex	$\Phi_{\text{decomp}}$ [%]
$[\text{Zn}(\text{m-L})_2]^a$	0.06
$[\text{Zn}(\text{p-L})_2]^a$	0.04
$[\text{Ru}(\text{bpy})_3]^{2+ b}$	0.005

<sup>a</sup>Determined in deaerated toluene by monitoring the photoluminescence intensity at 510 nm. <sup>b</sup>Determined in deaerated H<sub>2</sub>O by monitoring the emission intensity at 550 nm. Further details are in the SI on pages S43 and S44 (Figure S33).

magnitude lower, which is perhaps unsurprising given the substantial structural and electronic differences between these compound classes. In contrast to the 3d<sup>10</sup> Zn<sup>II</sup> compounds, the octahedral 4d<sup>6</sup> complex with Ru<sup>II</sup> benefits from a high ligand field stabilization energy, which decelerates ligand substitution reactions in the electronic ground state, and furthermore might affect the stability in excited states. The <sup>3</sup>ILCT excited states of the  $[\text{Zn}(\text{m-L})_2]$  and  $[\text{Zn}(\text{p-L})_2]$  complexes are considerably longer-lived ( $\tau_{\text{triplet}} = 38$  and 62  $\mu\text{s}$ , Table 1) than the <sup>3</sup>MLCT



excited state of  $[\text{Ru}(\text{bpy})_3]^{2+}$  ( $\tau_{\text{triplet}} < 1 \mu\text{s}$ ), which increases the likelihood of photo-decomposition in the  $\text{Zn}^{\text{II}}$  compounds.

Indeed, experiments in which the long-lived  $^3\text{ILCT}$  excited state of the  $\text{Zn}^{\text{II}}$  compounds is quenched partially by *trans*-stilbene indicate that under conditions of TTET catalysis,  $[\text{Zn}(m\text{-L})_2]$  and  $[\text{Zn}(p\text{-L})_2]$  are considerably more photorobust than in neat solvent without any substrate present (Figure 9). For instance, a neat  $3.2 \mu\text{M}$  solution of  $[\text{Zn}(p\text{-L})_2]$

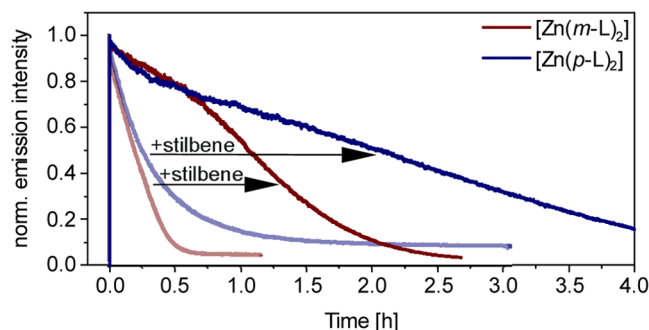


**Figure 9.** Influence of the addition of *trans*-stilbene on the photostability of  $[\text{Zn}(m\text{-L})_2]$  and  $[\text{Zn}(p\text{-L})_2]$  in deaerated toluene at 293 K. Red traces: Normalized intensity of the photoluminescence emitted by  $[\text{Zn}(m\text{-L})_2]$  at 510 nm in the absence (lighter trace) and presence of 10 mM *trans*-stilbene (darker trace). Blue traces: Analogous data set for  $[\text{Zn}(p\text{-L})_2]$ , with emission intensity monitoring at 490 nm, once without *trans*-stilbene (lighter trace) and once with 10 mM *trans*-stilbene (darker trace). All samples were irradiated with a 415 nm LED (7 W), combined with a 400 nm long-pass filter.

in deaerated toluene degraded essentially completely within 1.5 h of irradiation with a 415 nm LED providing 7 W of output power (light blue trace in Figure 9). Upon addition of 10 mM of *trans*-stilbene, it takes more than 4 h to reach a similar level of photodegradation (darker blue trace in Figure 9), and an analogous observation is made when comparing a neat toluene solution of  $10 \mu\text{M}$   $[\text{Zn}(m\text{-L})_2]$  with a mixture containing 10 mM *trans*-stilbene (red traces in Figure 9). These observations strongly suggest that photodegradation from the long-lived  $^3\text{ILCT}$  excited states is a major decomposition pathway in the  $[\text{Zn}(p\text{-L})_2]$  and  $[\text{Zn}(m\text{-L})_2]$  compounds, as suspected above (Figure 4). Since intersystem crossing is not quantitative in these  $\text{Zn}^{\text{II}}$  complexes (Table 1), it is possible to monitor their photodegradation by following their  $^1\text{ILCT}$  fluorescence intensities, even if the  $^3\text{ILCT}$  is quenched and primarily responsible for the photo-decomposition.

## CONCLUSIONS

The application potential of charge-transfer excited states in  $\text{Zn}^{\text{II}}$  complexes has so far remained underexplored in comparison to isoelectronic copper(I) coordination compounds.<sup>39,40</sup> Here, we demonstrate that intraligand charge-transfer (ILCT) excited states in tetrahedral  $\text{Zn}^{\text{II}}$  complexes can display similar reactivity as metal-to-ligand charge-transfer (MLCT) excited states in four-coordinate  $\text{Cu}^{\text{I}}$  compounds. In the latter, the photoactive MLCT excited states are typically strongly distorted due to the transient formation of a Jahn–Teller susceptible  $\text{Cu}^{\text{II}}$   $d^9$  metal species,<sup>78,113</sup> opening up unwanted nonradiative excited-state relaxation pathways. The ILCT excited states of the  $\text{Zn}^{\text{II}}$  complexes investigated herein do not suffer from this problem because the metal oxidation state remains unchanged. The  $\text{Zn}^{\text{II}}$  cation presumably

contributes to mediating intersystem crossing from the initially excited  $^1\text{ILCT}$  to the  $^3\text{ILCT}$  states, from where typical triplet photo-reactivity becomes accessible, including for example the photo-isomerization of olefins and the sensitization of triplet–triplet annihilation upconversion. The  $^3\text{ILCT}$  energies of our  $\text{Zn}^{\text{II}}$  complexes are sufficiently high to allow for upconversion from the blue to the ultraviolet spectral range, and these  $^3\text{ILCT}$  excited states are furthermore very reducing, making these  $\text{Zn}^{\text{II}}$  compounds strong photoreductants even in comparison to some of the well-established precious-metal-based systems.<sup>114</sup> Since the intersystem crossing is not quantitative, fluorescence from the  $^1\text{ILCT}$  excited state remains observable in our  $\text{Zn}^{\text{II}}$  compounds, in contrast to four-coordinate  $\text{Cu}^{\text{I}}$  complexes with photoactive MLCT states, in which intersystem crossing is usually ultrafast. Thus, our study illustrates some clear analogies and differences between tetrahedral  $\text{Zn}^{\text{II}}$  compounds with photoactive ILCT states and the more well-known four-coordinate  $\text{Cu}^{\text{I}}$  complexes.

The ILCT states of our  $\text{Zn}^{\text{II}}$  complexes complement the different types of photoactive excited states reported recently for first-row and other Earth-abundant transition-metal complexes,<sup>28</sup> which includes the classical MLCT states for  $d^6$  complexes ( $\text{Cr}^0$ ,  $\text{Mn}^{\text{I}}$ ,  $\text{Fe}^{\text{II}}$ ,  $\text{Co}^{\text{III}}$ ),<sup>19,24,25,115–117</sup> square-planar  $d^8$  compounds ( $\text{Ni}^{\text{II}}$ )<sup>26,118</sup> and four-coordinate  $d^{10}$  complexes ( $\text{Cu}^{\text{I}}$ ),<sup>3,78</sup> ligand-to-metal charge-transfer (LMCT) states for  $\text{Ti}^{\text{IV}}$ ,  $\text{Zr}^{\text{IV}}$ ,<sup>119,120</sup>  $\text{Mn}^{\text{IV}}$ ,  $\text{Fe}^{\text{III}}$  and  $\text{Co}^{\text{III}}$ ,<sup>121–126</sup> metal-centered (MC) states for  $\text{V}^{\text{III}}$ ,  $\text{Cr}^{\text{III}}$  and  $\text{Co}^{\text{III}}$ ,<sup>127–132</sup> as well as ligand-to-ligand charge-transfer (LLCT) excited states for two-coordinate  $\text{Cu}^{\text{I}}$  complexes.<sup>29–33</sup> Given these findings, it seems reasonable to conclude that  $\text{Zn}^{\text{II}}$  complexes with charge-transfer and triplet excited states would perhaps deserve greater attention in future studies aiming to discover new photophysics and photochemistry in first-row transition-metal complexes.

## METHODS

Chemicals were obtained from commercial suppliers in high purity and were used without further purification. Dry solvents were used as purchased from commercial suppliers or from an Innovative Technology PureSolv micro multiunit solvent purification system.

Nuclear magnetic resonance (NMR) spectroscopy was performed using either a 400 MHz Bruker Avance III spectrometer or a 600 MHz Bruker Avance III spectrometer at 298 K. The latter instrument was equipped with a direct observe 5 mm BBFO smart probe. Chemical shifts  $\delta$  are given in parts per million (ppm) and referenced to  $\text{CDCl}_3$  (7.26 ppm in  $^1\text{H}$ -NMR and 77.16 ppm in  $^{13}\text{C}$ -NMR spectroscopy),  $\text{CD}_2\text{Cl}_2$  (5.30 ppm in  $^1\text{H}$ -NMR and 53.84 ppm in  $^{13}\text{C}$ -NMR spectroscopy), or  $\text{DMSO}-d_6$  (2.50 ppm in  $^1\text{H}$ -NMR and 39.52 ppm in  $^{13}\text{C}$ -NMR spectroscopy).<sup>133</sup> The multiplicity of the signals is described with the following abbreviations: s (singlet), d (doublet), t (triplet), q (quartet), p (pentet), m (multiplet), and combinations of these abbreviations. The coupling constants  $J$  are given in hertz (Hz).

High-resolution mass spectroscopy (HRMS) was performed by Dr. Michael Pfeffer on a maxis 4G QTOF EDI spectrometer from Bruker. MALDI-TOF-MS was performed on a Bruker Microflex instrument operating in positive mode. The matrix (DCTB in  $\text{CH}_2\text{Cl}_2$ ) was evaporated onto the sample plate and then the substrate was evaporated onto the matrix.

Elemental analysis (EA) was performed by Sylvie Mittelheisser on a Vario Micro Cube instrument from Elementar. The amounts of carbon, hydrogen, and nitrogen were determined. All values are given in percentages.

Cyclic voltammetry was either performed in an MBraun glovebox under argon atmosphere using a Versastat4-200 potentiostat from Princeton Applied Research, or under deaerated conditions using a Versastat3-200 potentiostat from Princeton Applied Research.

Photocatalytic reactions were performed in NMR tubes with tube caps from VWR. The irradiation source was a SOLIS-415C high-power LED from ThorLabs with a 380 or 400 nm cutoff filter.

Photostabilities were measured using a SOLIS-415C high-power LED from ThorLabs with a 400 nm cutoff filter or a Roithner Lasertechnik GmbH 405 nm continuous-wave laser with an output power of 526 mW.

All photophysical measurements were carried out at 293 K and the solutions were purged with argon (4.8, PanGas) for at least 5 min using screw cap cuvettes. Steady-state optical absorption and UV–vis spectro-electrochemical measurements were recorded using a Cary 5000 spectrophotometer (Varian). Steady-state luminescence spectra were measured using a Fluorolog-3-22 instrument from Horiba Jobin-Yvon. Transient absorption and time-resolved absorption and emission measurements were performed on an LP920-KS instrument from Edinburgh Instruments. The excitation source was a pulsed Quantel Brilliant B Nd:YAG laser equipped with an optical parameter oscillator (OPO) from OPOTEK or a Nd:YAG laser (Quantel Q-smart 450 mJ, ca. 10 ns pulse width) with a beam expander (BE02-355 from Thorlabs). The transient absorption spectra were detected on an iCCD camera (Andor), while kinetics at a single wavelength were recorded with a photomultiplier tube. Fluorescence lifetimes were measured on a LifeSpec II spectrometer (time-correlated single photon counting technique) from Edinburgh Instruments using picosecond pulsed diode lasers for excitation at 405 nm.

## ■ ASSOCIATED CONTENT

### SI Supporting Information

The Supporting Information is available free of charge at <https://pubs.acs.org/doi/10.1021/jacsau.2c00442>.

Materials and methods, synthetic procedures and characterization data, electrochemical data, spectroscopic data, and additional information to photophysical measurements and stability (PDF)

## ■ AUTHOR INFORMATION

### Corresponding Author

Oliver S. Wenger – Department of Chemistry, University of Basel, 4056 Basel, Switzerland; [orcid.org/0000-0002-0739-0553](https://orcid.org/0000-0002-0739-0553); Email: [oliver.wenger@unibas.ch](mailto:oliver.wenger@unibas.ch)

### Authors

Jasmin A. Kübler – Department of Chemistry, University of Basel, 4056 Basel, Switzerland

Björn Pfund – Department of Chemistry, University of Basel, 4056 Basel, Switzerland; [orcid.org/0000-0003-0936-2975](https://orcid.org/0000-0003-0936-2975)

Complete contact information is available at: <https://pubs.acs.org/10.1021/jacsau.2c00442>

### Author Contributions

The manuscript was written through contributions of all authors. All authors have given approval to the final version of the manuscript.

### Notes

The authors declare no competing financial interest.

## ■ ACKNOWLEDGMENTS

This work was supported by the Swiss National Science Foundation through the NCCR Molecular Systems Engineering and through grant number 200020\_207329. B.P. acknowledges a fellowship from the National Research Fund,

Luxembourg (Ph.D. Grant 14583224). Han Li is thanked for the synthesis of the annihilator.

## ■ REFERENCES

- (1) Dietrich-Buchecker, C. O.; Marnot, P. A.; Sauvage, J. P.; Kirchhoff, J. R.; McMillin, D. R. Bis(2,9-Diphenyl-1,10-Phenanthroline)Copper(I): A Copper Complex with a Long-Lived Charge-Transfer Excited State. *J. Chem. Soc., Chem. Commun.* **1983**, 513–515.
- (2) Cuttall, D. G.; Kuang, S. M.; Fanwick, P. E.; McMillin, D. R.; Walton, R. A. Simple Cu(I) Complexes with Unprecedented Excited-State Lifetimes. *J. Am. Chem. Soc.* **2002**, *124*, 6–7.
- (3) Lazorski, M. S.; Castellano, F. N. Advances in the Light Conversion Properties of Cu(I)-Based Photosensitizers. *Polyhedron* **2014**, *82*, 57–70.
- (4) Costa, R. D.; Ortí, E.; Bolink, H. J.; Monti, F.; Accorsi, G.; Armaroli, N. Luminescent Ionic Transition-Metal Complexes for Light-Emitting Electrochemical Cells. *Angew. Chem., Int. Ed.* **2012**, *51*, 8178–8211.
- (5) Czerwieniec, R.; Leitzl, M. J.; Homeier, H. H. H.; Yersin, H. Cu(I) Complexes – Thermally Activated Delayed Fluorescence. Photophysical Approach and Material Design. *Coord. Chem. Rev.* **2016**, *325*, 2–28.
- (6) Bizzarri, C.; Spuling, E.; Knoll, D. M.; Volz, D.; Bräse, S. Sustainable Metal Complexes for Organic Light-Emitting Diodes (OLEDs). *Coord. Chem. Rev.* **2018**, *373*, 49–82.
- (7) Doettinger, F.; Yang, Y.; Schmid, M. A.; Frey, W.; Karnahl, M.; Tschierlei, S. Cross-Coupled Phenyl- and Alkynyl-Based Phenanthrolines and Their Effect on the Photophysical and Electrochemical Properties of Heteroleptic Cu(I) Photosensitizers. *Inorg. Chem.* **2021**, *60*, 5391–5401.
- (8) Housecroft, C. E.; Constable, E. C. The Emergence of Copper(I)-Based Dye Sensitized Solar Cells. *Chem. Soc. Rev.* **2015**, *44*, 8386–8398.
- (9) Reiser, O. Shining Light on Copper: Unique Opportunities for Visible-Light-Catalyzed Atom Transfer Radical Addition Reactions and Related Processes. *Acc. Chem. Res.* **2016**, *49*, 1990–1996.
- (10) Hossain, A.; Bhattacharyya, A.; Reiser, O. Copper's Rapid Ascent in Visible-Light Photoredox Catalysis. *Science* **2019**, *364*, No. eaav9713.
- (11) Nicholls, T. P.; Constable, G. E.; Robertson, J. C.; Gardiner, M. G.; Bissember, A. C. Brønsted Acid Cocatalysis in Copper(I)-Photocatalyzed  $\alpha$ -Amino C-H Bond Functionalization. *ACS Catal.* **2016**, *6*, 451–457.
- (12) Jacob, C.; Baguia, H.; Dubart, A.; Oger, S.; Thilmany, P.; Beaudelot, J.; Deldaele, C.; Peruško, S.; Landrain, Y.; Michelet, B.; Neale, S.; Romero, E.; Moucheron, C.; Van Speybroeck, V.; Theunissen, C.; Evano, G. A General Synthesis of Azetidines by Copper-Catalyzed Photoinduced Anti-Baldwin Radical Cyclization of Ynamides. *Nat. Commun.* **2022**, *13*, No. 560.
- (13) Minozzi, C.; Caron, A.; Grenier-Petel, J. C.; Santandrea, J.; Collins, S. K. Heteroleptic Copper(I)-Based Complexes for Photocatalysis: Combinatorial Assembly, Discovery, and Optimization. *Angew. Chem., Int. Ed.* **2018**, *57*, 5477–5481.
- (14) Eberhart, M. S.; Phelan, B. T.; Niklas, J.; Sprague-Klein, E. A.; Kaphan, D. M.; Gosztola, D. J.; Chen, L. X.; Tiede, D. M.; Poluektov, O. G.; Mulfort, K. L. Surface Immobilized Copper(I) Diimine Photosensitizers as Molecular Probes for Elucidating the Effects of Confinement at Interfaces for Solar Energy Conversion. *Chem. Commun.* **2020**, *56*, 12130–12133.
- (15) Hayes, D.; Kohler, L.; Chen, L. X.; Mulfort, K. L. Ligand Mediation of Vectorial Charge Transfer in Cu(I)Diimine Chromophore-Acceptor Dyads. *J. Phys. Chem. Lett.* **2018**, *9*, 2070–2076.
- (16) Argüello Cordero, M. A.; Boden, P. J.; Rentschler, M.; Di Martino-Fumo, P.; Frey, W.; Yang, Y.; Gerhards, M.; Karnahl, M.; Lochbrunner, S.; Tschierlei, S. Comprehensive Picture of the Excited State Dynamics of Cu(I)- and Ru(II)-Based Photosensitizers with Long-Lived Triplet States. *Inorg. Chem.* **2022**, *61*, 214–226.

- (17) Armaroli, N. Photoactive Mono- and Polynuclear Cu(I)-Phenanthrolines. A Viable Alternative to Ru(II)-Polypyridines? *Chem. Soc. Rev.* **2001**, *30*, 113–124.
- (18) Förster, C.; Heinze, K. Photophysics and Photochemistry with Earth-Abundant Metals-Fundamentals and Concepts. *Chem. Soc. Rev.* **2020**, *49*, 1057–1070.
- (19) Sinha, N.; Pfund, B.; Wegeberg, C.; Prescimone, A.; Wenger, O. S. Cobalt(III) Carbene Complex with an Electronic Excited-State Structure Similar to Cyclometalated Iridium(III) Compounds. *J. Am. Chem. Soc.* **2022**, *144*, 9859–9873.
- (20) Paulus, B. C.; Adelman, S. L.; Jamula, L. L.; McCusker, J. K. Leveraging Excited-State Coherence for Synthetic Control of Ultrafast Dynamics. *Nature* **2020**, *582*, 214–218.
- (21) Liu, Y.; Persson, P.; Sundström, V.; Wärnmark, K. Fe N-Heterocyclic Carbene Complexes as Promising Photosensitizers. *Acc. Chem. Res.* **2016**, *49*, 1477–1485.
- (22) Zhang, W.; Gaffney, K. J. Mechanistic Studies of Photoinduced Spin Crossover and Electron Transfer in Inorganic Complexes. *Acc. Chem. Res.* **2015**, *48*, 1140–1148.
- (23) Cebrián, C.; Pastore, M.; Monari, A.; Assfeld, X.; Gros, P. C.; Haacke, S. Ultrafast Spectroscopy of Fe(II) Complexes Designed for Solar-Energy Conversion: Current Status and Open Questions. *ChemPhysChem* **2022**, *23*, No. e202100659.
- (24) Herr, P.; Kerzig, C.; Larsen, C. B.; Häussinger, D.; Wenger, O. S. Manganese(I) Complexes with Metal-to-Ligand Charge Transfer Luminescence and Photoreactivity. *Nat. Chem.* **2021**, *13*, 956–962.
- (25) Wegeberg, C.; Häussinger, D.; Wenger, O. S. Pyrene-Decoration of a Chromium(0) Tris(Diisocyanide) Enhances Excited State Delocalization: A Strategy to Improve the Photoluminescence of 3d<sup>6</sup> Metal Complexes. *J. Am. Chem. Soc.* **2021**, *143*, 15800–15811.
- (26) Ting, S. I.; Garakyaraghi, S.; Taliaferro, C. M.; Shields, B. J.; Scholes, G. D.; Castellano, F. N.; Doyle, A. G. <sup>3</sup>d-d Excited States of Ni(II) Complexes Relevant to Photoredox Catalysis: Spectroscopic Identification and Mechanistic Implications. *J. Am. Chem. Soc.* **2020**, *142*, 5800–5810.
- (27) Tian, L.; Till, N. A.; Kudisch, B.; MacMillan, D. W. C.; Scholes, G. D. Transient Absorption Spectroscopy Offers Mechanistic Insights for an Iridium/Nickel-Catalyzed C-O Coupling. *J. Am. Chem. Soc.* **2020**, *142*, 4555–4559.
- (28) Wegeberg, C.; Wenger, O. S. Luminescent First-Row Transition Metal Complexes. *JACS Au* **2021**, *1*, 1860–1876.
- (29) Hamze, R.; Peltier, J. L.; Sylvinson, D.; Jung, M.; Cardenas, J.; Haiges, R.; Soleilhavoup, M.; Jazzar, R.; Djurovich, P. I.; Bertrand, G.; Thompson, M. E. Eliminating Nonradiative Decay in Cu(I) Emitters: >99% Quantum Efficiency and Microsecond Lifetime. *Science* **2019**, *363*, 601–606.
- (30) Di, D.; Romanov, A. S.; Yang, L.; Richter, J. M.; Rivett, J. P. H.; Jones, S.; Thomas, T. H.; Jalebi, M. A.; Friend, R. H.; Linnolahti, M.; Bochmann, M.; Credginton, D. High-Performance Light-Emitting Diodes Based on Carbene-Metal-Amides. *Science* **2017**, *356*, 159–163.
- (31) Gernert, M.; Müller, U.; Haehnel, M.; Pflaum, J.; Steffen, A. A Cyclic Alkyl(Amino)Carbene as Two-Atom  $\pi$ -Chromophore Leading to the First Phosphorescent Linear Cu<sup>I</sup> Complexes. *Chem. - Eur. J.* **2017**, *23*, 2206–2216.
- (32) Gernert, M.; Balles-Wolf, L.; Kerner, F.; Müller, U.; Schmiedel, A.; Holzapfel, M.; Marian, C. M.; Pflaum, J.; Lambert, C.; Steffen, A. Cyclic (Amino)(Aryl)Carbenes Enter the Field of Chromophore Ligands: Expanded  $\pi$  System Leads to Unusually Deep Red Emitting Cu<sup>I</sup> Compounds. *J. Am. Chem. Soc.* **2020**, *142*, 8897–8909.
- (33) Shi, S.; Jung, M. C.; Coburn, C.; Tadde, A.; Sylvinson, D. M. R.; Djurovich, P. I.; Forrest, S. R.; Thompson, M. E. Highly Efficient Photo- and Electroluminescence from Two-Coordinate Cu(I) Complexes Featuring Nonconventional N-Heterocyclic Carbenes. *J. Am. Chem. Soc.* **2019**, *141*, 3576–3588.
- (34) Wang, S. Luminescence and Electroluminescence of Al(III), B(III), Be(II) and Zn(II) Complexes with Nitrogen Donors. *Coord. Chem. Rev.* **2001**, *215*, 79–98.
- (35) Kunkely, H.; Vogler, A. Absorption and Emission Spectrum of [Zn<sub>4</sub>O(Acetate)<sub>6</sub>]. *J. Chem. Soc., Chem. Commun.* **1990**, *40*, 1204–1205.
- (36) Lee, C.-F.; Chin, K.-F.; Peng, S.-M.; Che, C.-M. A Luminescent Tetrameric Zinc(II) Complex Containing the 7-Azaindolate Ligand. Photophysical Properties and Crystal Structure. *J. Chem. Soc., Dalton Trans.* **1993**, 467–470.
- (37) Kurz, H.; Hörner, G.; Weser, O.; Li Manni, G.; Weber, B. Quenched Lewis Acidity: Studies on the Medium Dependent Fluorescence of Zinc(II) Complexes. *Chem. - Eur. J.* **2021**, *27*, 15159–15171.
- (38) Consiglio, G.; Oliveri, I. P.; Cacciola, S.; Maccarrone, G.; Failla, S.; Di Bella, S. Dinuclear Zinc(II) Salen-Type Schiff-Base Complexes as Molecular Tweezers. *Dalton Trans.* **2020**, *49*, 5121–5133.
- (39) Tabone, R.; Feser, D.; Lemma, E. D.; Schepers, U.; Bizzarri, C. Intriguing Heteroleptic Zn<sup>II</sup> Bis(Dipyrrinato) Emitters in the Far-Red Region With Large Pseudo-Stokes Shift for Bioimaging. *Front. Chem.* **2021**, *9*, No. 754420.
- (40) Tungulin, D.; Leier, J.; Carter, A. B.; Powell, A. K.; Albuquerque, R. Q.; Unterreiner, A. N.; Bizzarri, C. Chasing BODIPY: Enhancement of Luminescence in Homoleptic Bis-(Dipyrrinato) Zn<sup>II</sup> Complexes Utilizing Symmetric and Unsymmetrical Dipyrrins. *Chem. - Eur. J.* **2019**, *25*, 3816–3827.
- (41) Kusaka, S.; Sakamoto, R.; Kitagawa, Y.; Okumura, M.; Nishihara, H. An Extremely Bright Heteroleptic Bis(Dipyrrinato)-Zinc(II) Complex. *Chem. - Asian J.* **2012**, *7*, 907–910.
- (42) Filatov, M. A.; Lebedev, A. Y.; Mukhin, S. N.; Vinogradov, S. A.; Cheprakov, A. V.  $\Pi$ -Extended Dipyrrins Capable of Highly Fluorogenic Complexation With Metal Ions. *J. Am. Chem. Soc.* **2010**, *132*, 9552–9554.
- (43) Sakamoto, R.; Iwashima, T.; Kögel, J. F.; Kusaka, S.; Tsuchiya, M.; Kitagawa, Y.; Nishihara, H. Dissymmetric Bis(Dipyrrinato)Zinc(II) Complexes: Rich Variety and Bright Red to Near-Infrared Luminescence with a Large Pseudo-Stokes Shift. *J. Am. Chem. Soc.* **2016**, *138*, 5666–5677.
- (44) Karges, J.; Blacque, O.; Chao, H.; Gasser, G. Polymeric Bis(Dipyrrinato) Zinc(II) Nanoparticles as Selective Imaging Probes for Lysosomes of Cancer Cells. *Inorg. Chem.* **2019**, *58*, 12422–12432.
- (45) Tsuchiya, M.; Sakamoto, R.; Shimada, M.; Yamanoi, Y.; Hattori, Y.; Sugimoto, K.; Nishibori, E.; Nishihara, H. Bis-(Dipyrrinato)Zinc(II) Complexes: Emission in the Solid State. *Inorg. Chem.* **2016**, *55*, 5732–5734.
- (46) Yu, G.; Yin, S.; Liu, Y.; Shuai, Z.; Zhu, D. Structures, Electronic States, and Electroluminescent Properties of a Zinc(II) 2-(2-Hydroxyphenyl)Benzothiazolate Complex. *J. Am. Chem. Soc.* **2003**, *125*, 14816–14824.
- (47) Roh, S. G.; Kim, Y. H.; Seo, K. D.; Lee, D. H.; Kim, H. K.; Park, Y. I.; Park, J. W.; Lee, J. H. Synthesis, Photophysical, and Electroluminescent Device Properties of Zn(II)-Chelated Complexes Based on Functionalized Benzothiazole Derivatives. *Adv. Funct. Mater.* **2009**, *19*, 1663–1671.
- (48) Li, Z.; Dellali, A.; Malik, J.; Motevalli, M.; Nix, R. M.; Olukoya, T.; Peng, Y.; Ye, H.; Gillin, W. P.; Hernández, I.; Wyatt, P. B. Luminescent Zinc(II) Complexes of Fluorinated Benzothiazol-2-Yl Substituted Phenoxide and Enolate Ligands. *Inorg. Chem.* **2013**, *52*, 1379–1387.
- (49) Ardizzioia, G. A.; Colombo, G.; Therrien, B.; Brenna, S. Tuning the Fluorescence Emission and HOMO-LUMO Band Gap in Homoleptic Zinc(II) Complexes with N,O-Bidentate (Imidazo[1,5-a]Pyrid-3-Yl)Phenols. *Eur. J. Inorg. Chem.* **2019**, *2019*, 1825–1831.
- (50) Borisov, S. M.; Pommer, R.; Svec, J.; Peters, S.; Novakova, V.; Klimant, I. New Red-Emitting Schiff Base Chelates: Promising Dyes for Sensing and Imaging of Temperature and Oxygen via Phosphorescence Decay Time. *J. Mater. Chem. C* **2018**, *6*, 8999–9009.
- (51) Bestgen, S.; Schoo, C.; Neumeier, B. L.; Feuerstein, T. J.; Zovko, C.; Köppe, R.; Feldmann, C.; Roesky, P. W. Intensely Photoluminescent Diamidophosphines of the Alkaline-Earth Metals, Aluminum, and Zinc. *Angew. Chem., Int. Ed.* **2018**, *57*, 14265–14269.



- (52) Wang, R.; Deng, L.; Fu, M.; Cheng, J.; Li, J. Novel Zn<sup>II</sup> Complexes of 2-(2-Hydroxyphenyl)Benzothiazoles Ligands: Electroluminescence and Application as Host Materials for Phosphorescent Organic Light-Emitting Diodes. *J. Mater. Chem.* **2012**, *22*, 23454–23460.
- (53) Sapochak, L. S.; Benincasa, F. E.; Schofield, R. S.; Baker, J. L.; Riccio, K. K. C.; Fogarty, D.; Kohlmann, H.; Ferris, K. F.; Burrows, P. E. Electroluminescent Zinc(II) Bis(8-Hydroxyquinoline): Structural Effects on Electronic States and Device Performance. *J. Am. Chem. Soc.* **2002**, *124*, 6119–6125.
- (54) Liu, S. F.; Wu, Q.; Schmider, H. L.; Aziz, H.; Hu, N. X.; Popović, Z.; Wang, S. Syntheses, Structures, and Electroluminescence of New Blue/Green Luminescent Chelate Compounds: Zn(2-Py-in)<sub>2</sub>(THF), BPh<sub>2</sub>(2-Py-in), Be(2-Py-in)<sub>2</sub>, and BPh<sub>2</sub>(2-Py-Aza) [2-Py-in = 2-(2-Pyridyl)Indole; 2-py-aza = 2-(2-pyridyl)-7-azaindole]. *J. Am. Chem. Soc.* **2000**, *122*, 3671–3678.
- (55) Cheng, G.; So, G. K. M.; To, W. P.; Chen, Y.; Kwok, C. C.; Ma, C.; Guan, X.; Chang, X.; Kwok, W. M.; Che, C. M. Luminescent Zinc(II) and Copper(I) Complexes for High-Performance Solution-Processed Monochromatic and White Organic Light-Emitting Devices. *Chem. Sci.* **2015**, *6*, 4623–4635.
- (56) Son, H.-J.; Han, W.; Chun, J.; Kang, B.; Kwon, S.; Ko, J.; Han, S. J.; Lee, C.; Kim, S. J.; Kang, S. O. Generation of Blue Light-Emitting Zinc Complexes by Band-Gap Control of the Oxazolyphenolate Ligand System: Syntheses, Characterizations, and Organic Light Emitting Device Applications of 4-Coordinated Bis(2-Oxazolyphenolate) Zinc(II) Complexes. *Inorg. Chem.* **2008**, *47*, 5666–5676.
- (57) Xu, H.; Xu, Z. F.; Yue, Z. Y.; Yan, P. F.; Wang, B.; Jia, L. W.; Li, G. M.; Sun, W. B.; Zhang, J. W. A Novel Deep Blue-Emitting Zn<sup>II</sup> Complex Based on Carbazole-Modified 2-(2-Hydroxyphenyl)-Benzimidazole: Synthesis, Bright Electroluminescence, and Substitution Effect on Photoluminescent, Thermal, and Electrochemical Properties. *J. Phys. Chem. C* **2008**, *112*, 15517–15525.
- (58) Kögel, J. F.; Kusaka, S.; Sakamoto, R.; Iwashima, T.; Tsuchiya, M.; Toyoda, R.; Matsuoka, R.; Tsukamoto, T.; Yuasa, J.; Kitagawa, Y.; Kawai, T.; Nishihara, H. Heteroleptic [Bis(Oxazoline)](Dipyrrinato)-Zinc(II) Complexes: Bright and Circularly Polarized Luminescence from an Originally Achiral Dipyrrinato Ligand. *Angew. Chem.* **2016**, *128*, 1399–1403.
- (59) Pang, J.; Marcotte, E. J. P.; Seward, C.; Brown, R. S.; Wang, S. A Blue Luminescent Star-Shaped Zn<sup>II</sup> Complex That Can Detect Benzene. *Angew. Chem.* **2001**, *113*, 4166–4169.
- (60) Xie, D.; Jing, J.; Cai, Y. B.; Tang, J.; Chen, J. J.; Zhang, J. L. Construction of an Orthogonal ZnSalen/Salophen Library as a Colour Palette for One- and Two-Photon Live Cell Imaging. *Chem. Sci.* **2014**, *5*, 2318–2327.
- (61) Xu, B.; Chi, Z.; Zhang, X.; Li, H.; Chen, C.; Liu, S.; Zhang, Y.; Xu, J. A New Ligand and Its Complex with Multi-Stimuli-Responsive and Aggregation-Induced Emission Effects. *Chem. Commun.* **2011**, *47*, 11080–11082.
- (62) Marafie, J. A.; Bradley, D. D. C.; Williams, C. K. Thermally Stable Zinc Disalphen Macrocycles Showing Solid-State and Aggregation-Induced Enhanced Emission. *Inorg. Chem.* **2017**, *56*, 5688–5695.
- (63) Singh, K.; Siddiqui, I.; Sridharan, V.; Kumar Yadav, R. A.; Jou, J. H.; Adhikari, D. Aggregation-Induced Enhanced Emission-Active Zinc(II)  $\beta$ -Diketiminato Complexes Enabling High-Performance Solution-Processable OLEDs. *Inorg. Chem.* **2021**, *60*, 19128–19135.
- (64) Evans, D. A.; Lee, L. M.; Vargas-Baca, I.; Cowley, A. H. Photophysical Tuning of the Aggregation-Induced Emission of a Series of Para-Substituted Aryl Bis(Imino)Acenaphthene Zinc Complexes. *Dalton Trans.* **2015**, *44*, 11984–11996.
- (65) Cibian, M.; Shahalizad, A.; Souissi, F.; Castro, J.; Ferreira, J. G.; Chartrand, D.; Nunzi, J. M.; Hanan, G. S. A Zinc(II) Benzamidinate N-Oxide Complex as an Aggregation-Induced Emission Material: Toward Solution-Processable White Organic Light-Emitting Devices. *Eur. J. Inorg. Chem.* **2018**, *2018*, 4322–4330.
- (66) Sakai, Y.; Sagara, Y.; Nomura, H.; Nakamura, N.; Suzuki, Y.; Miyazaki, H.; Adachi, C. Zinc Complexes Exhibiting Highly Efficient Thermally Activated Delayed Fluorescence and Their Application to Organic Light-Emitting Diodes. *Chem. Commun.* **2015**, *51*, 3181–3184.
- (67) Xiong, J.; Li, K.; Teng, T.; Chang, X.; Wei, Y.; Wu, C.; Yang, C. Dinuclear Zn<sup>II</sup> Complexes Exhibiting Thermally Activated Delayed Fluorescence and Luminescence Polymorphism. *Chem. - Eur. J.* **2020**, *26*, 6887–6893.
- (68) Berezin, A. S.; Vinogradova, K. A.; Krivopalov, V. P.; Nikolaenkova, E. B.; Plyusnin, V. F.; Kupryakov, A. S.; Pervukhina, N. V.; Naumov, D. Y.; Bushuev, M. B. Excitation-Wavelength-Dependent Emission and Delayed Fluorescence in a Proton-Transfer System. *Chem. - Eur. J.* **2018**, *24*, 12790–12795.
- (69) Goswami, B.; Feuerstein, T. J.; Yadav, R.; Lebedkin, S.; Boden, P. J.; Steiger, S. T.; Niedner-Schatteburg, G.; Gerhards, M.; Kappes, M. M.; Roesky, P. W. Thermally Activated Delayed Fluorescence and Phosphorescence Quenching in Iminophosphonamide Copper and Zinc Complexes. *Chem. - Eur. J.* **2021**, *27*, 15110–15118.
- (70) Mrózek, O.; Gernert, M.; Belyaev, A.; Mitra, M.; Janiak, L.; Marian, C. M.; Steffen, A. Ultra-long Lived Luminescent Triplet Excited States in Cyclic (Alkyl)(Amino)Carbene Complexes of Zn(II) Halides. *Chem. - Eur. J.* **2022**, *28*, No. e202201114.
- (71) Temerova, D.; Kisel, K. S.; Eskelinen, T.; Melnikov, A. S.; Kinnunen, N.; Hirva, P.; Shakirova, J. R.; Tunik, S. P.; Grachova, E. V.; Koshevoy, I. O. Diversifying the Luminescence of Phenanthro-Diimine Ligands in Zinc Complexes. *Inorg. Chem. Front.* **2021**, *8*, 2549–2560.
- (72) Ferraro, V.; Baggio, F.; Castro, J.; Bortoluzzi, M. Green Phosphorescent Zn(II) Halide Complexes with N,N,N',N'-Tetramethyl-P-Indol-1-Yl Phosphonic Diamide as Ligand. *Eur. J. Inorg. Chem.* **2022**, *2022*, No. e202200119.
- (73) Strieth-Kalthoff, F.; Glorius, F. Triplet Energy Transfer Photocatalysis: Unlocking the Next Level. *Chem* **2020**, *6*, 1888–1903.
- (74) Bharmoria, P.; Bildirir, H.; Moth-Poulsen, K. Triplet-Triplet Annihilation Based near Infrared to Visible Molecular Photon Upconversion. *Chem. Soc. Rev.* **2020**, *49*, 6529–6554.
- (75) Marzo, L.; Pagire, S. K.; Reiser, O.; König, B. Visible-Light Photocatalysis: Does It Make a Difference in Organic Synthesis? *Angew. Chem., Int. Ed.* **2018**, *57*, 10034–10072.
- (76) Magnuson, A.; Anderlund, M.; Johansson, O.; Lindblad, P.; Lomoth, R.; Polivka, T.; Ott, S.; Stensjö, K.; Styring, S.; Sundström, V.; Hammarström, L. Biomimetic and Microbial Approaches to Solar Fuel Generation. *Acc. Chem. Res.* **2009**, *42*, 1899–1909.
- (77) Wenger, O. S. Photoactive Complexes with Earth-Abundant Metals. *J. Am. Chem. Soc.* **2018**, *140*, 13522–13533.
- (78) Chen, L. X.; Shaw, G. B.; Novozhilova, I.; Liu, T.; Jennings, G.; Attenkofer, K.; Meyer, G. J.; Coppens, P. MLCT State Structure and Dynamics of a Copper(I) Diimine Complex Characterized by Pump-Probe X-Ray and Laser Spectroscopies and DFT Calculations. *J. Am. Chem. Soc.* **2003**, *125*, 7022–7034.
- (79) Kohler, L.; Hadt, R. G.; Hayes, D.; Chen, L. X.; Mulfort, K. L. Synthesis, Structure, and Excited State Kinetics of Heteroleptic Cu(I) Complexes with a New Sterically Demanding Phenanthroline Ligand. *Dalton Trans.* **2017**, *46*, 13088–13100.
- (80) Zhao, X.; Zhao, J. Long-Lived Charge Separated State and Thermally Activated Delayed Fluorescence in Anthraquinone-Phenoxazine Electron Donor-Acceptor Dyads. *Chem. Commun.* **2022**, *58*, 7666–7669.
- (81) Ledger, M. B.; Salmon, G. A. Triplet-Triplet Extinction Coefficients of Anthracene and 9-Bromoanthracene Determined by a Ground State Depletion Method. *J. Chem. Soc., Faraday Trans. 2* **1976**, *72*, 883–886.
- (82) Müller, P.; Brettel, K. [Ru(Bpy)<sub>3</sub>]<sup>2+</sup> as a Reference in Transient Absorption Spectroscopy: Differential Absorption Coefficients for Formation of the Long-Lived <sup>3</sup>MLCT Excited State. *Photochem. Photobiol. Sci.* **2012**, *11*, 632–636.
- (83) Dong, Y.; Kumar, P.; Maity, P.; Kurganskii, I.; Li, S.; Elmali, A.; Zhao, J.; Escudero, D.; Wu, H.; Karatay, A.; Mohammed, O. F.;

- Fedin, M. Twisted BODIPY Derivative: Intersystem Crossing, Electron Spin Polarization and Application as a Novel Photodynamic Therapy Reagent. *Phys. Chem. Chem. Phys.* **2021**, *23*, 8641–8652.
- (84) Montalti, M.; Credi, A.; Prodi, L.; Gandolfi, M. T. *Handbook of Photochemistry*, 3rd ed.; CRC/Taylor & Francis: Boca Raton, 2006.
- (85) Pang, J.; Deng, Z.; Sun, S.; Huang, G.; Zhang, G.; Islam, A.; Dang, L.; Phillips, D. L.; Li, M.-D. Unprecedentedly Ultrafast Dynamics of Excited States of C=C Photoswitching Molecules in Nanocrystals and Microcrystals. *J. Phys. Chem. Lett.* **2021**, *12*, 41–48.
- (86) Kovalenko, S. A.; Dobryakov, A. L.; Ioffe, I.; Ernstring, N. P. Evidence for the Phantom State in Photoinduced Cis-Trans Isomerization of Stilbene. *Chem. Phys. Lett.* **2010**, *493*, 255–258.
- (87) Singh, C.; Ghosh, R.; Mondal, J. A.; Palit, D. K. Excited State Dynamics of a Push-Pull Stilbene: A Femtosecond Transient Absorption Spectroscopic Study. *J. Photochem. Photobiol., A* **2013**, *263*, 50–60.
- (88) Patra, T.; Mukherjee, S.; Ma, J.; Strieth-Kalthoff, F.; Glorius, F. Visible-Light-Photosensitized Aryl and Alkyl Decarboxylative Functionalization Reactions. *Angew. Chem.* **2019**, *131*, 10624–10630.
- (89) Ohkubo, K.; Suga, K.; Morikawa, K.; Fukuzumi, S. Selective Oxygenation of Ring-Substituted Toluene with Electron-Donating and -Withdrawing Substituents by Molecular Oxygen via Photoinduced Electron Transfer. *J. Am. Chem. Soc.* **2003**, *125*, 12850–12859.
- (90) Cyr, D.; Das, P. Kinetics of C-C and C-H Bond Cleavage in Phenyl Alkane Radical Cations Generated by Photoinduced Electron Transfer. *J. Phys. Chem. A* **2014**, *118*, 11155–11167.
- (91) Shukla, D.; Young, R. H.; Farid, S. Reducing Power of Photogenerated  $\alpha$ -Hydroxy Radicals. Proton-Coupled Electron Transfer. *J. Phys. Chem. A* **2004**, *108*, 10386–10394.
- (92) Heckmann, A.; Lambert, C. Organic Mixed-Valence Compounds: A Playground for Electrons and Holes. *Angew. Chem., Int. Ed.* **2012**, *51*, 326–392.
- (93) Singh-Rachford, T. N.; Castellano, F. N. Photon Upconversion Based on Sensitized Triplet-Triplet Annihilation. *Coord. Chem. Rev.* **2010**, *254*, 2560–2573.
- (94) Sanders, S. N.; Schloemer, T. H.; Gangishetty, M. K.; Anderson, D.; Seitz, M.; Gallegos, A. O.; Stokes, R. C.; Congreve, D. N. Triplet Fusion Upconversion Nanocapsules for Volumetric 3D Printing. *Nature* **2022**, *604*, 474–478.
- (95) Imperiale, C. J.; Green, P. B.; Hasham, M.; Wilson, M. W. B. Ultra-Small PbS Nanocrystals as Sensitizers for Red-to-Blue Triplet-Fusion Upconversion. *Chem. Sci.* **2021**, *12*, 14111–14120.
- (96) Yang, M.; Sheykhi, S.; Zhang, Y.; Milsmann, C.; Castellano, F. N. Low Power Threshold Photochemical Upconversion Using a Zirconium(IV) LMCT Photosensitizer. *Chem. Sci.* **2021**, *12*, 9069–9077.
- (97) Uji, M.; Harada, N.; Kimizuka, N.; Saigo, M.; Miyata, K.; Onda, K.; Yanai, N. Heavy Metal-Free Visible-to-UV Photon Upconversion with over 20% Efficiency Sensitized by a Ketocoumarin Derivative. *J. Mater. Chem. C* **2022**, *10*, 4558–4562.
- (98) Harada, N.; Sasaki, Y.; Hosoyamada, M.; Kimizuka, N.; Yanai, N. Discovery of Key TIPS-Naphthalene for Efficient Visible-to-UV Photon Upconversion under Sunlight and Room Light. *Angew. Chem., Int. Ed.* **2021**, *60*, 142–147.
- (99) VanOrman, Z. A.; Nienhaus, L. Feeling Blue No More: How TIPS-Naphthalene Enables Efficient Visible-to-UV Upconversion. *Matter* **2021**, *4*, 2625–2626.
- (100) Zähringer, T. J. B.; Bertrams, M. S.; Kerzig, C. Purely Organic Vis-to-UV Upconversion with an Excited Annihilator Singlet beyond 4 eV. *J. Mater. Chem. C* **2022**, *10*, 4568–4573.
- (101) Olesund, A.; Johansson, J.; Edhborg, F.; Ghasemi, S.; Moth-Poulsen, K.; Albinsson, B. Approaching the Spin-Statistical Limit in Visible-to-Ultraviolet Photon Upconversion. *J. Am. Chem. Soc.* **2022**, *144*, 3706–3716.
- (102) Schmid, L.; Glaser, F.; Schaer, R.; Wenger, O. S. High Triplet Energy Iridium(III) Isocyanoborato Complex for Photochemical Upconversion, Photoredox and Energy Transfer Catalysis. *J. Am. Chem. Soc.* **2022**, *144*, 963–976.
- (103) Grundke, C.; Silva, R. C.; Kitzmann, W. R.; Heinze, K.; De Oliveira, K. T.; Opatz, T. Photochemical  $\alpha$ -Aminonitrile Synthesis Using Zn-Phthalocyanines as Near-Infrared Photocatalysts. *J. Org. Chem.* **2022**, *87*, 5630–5642.
- (104) Felter, K. M.; Fravventura, M. C.; Koster, E.; Abellon, R. D.; Savenije, T. J.; Grozema, F. C. Solid-State Infrared Upconversion in Perylene Diimides Followed by Direct Electron Injection. *ACS Energy Lett.* **2020**, *5*, 124–129.
- (105) Mahmood, Z.; Rehmat, N.; Ji, S.; Zhao, J.; Sun, S.; Di Donato, M.; Li, M.; Teddei, M.; Huo, Y. Tuning the Triplet Excited State of Bis(Dipyrrin) Zinc(II) Complexes: Symmetry Breaking Charge Transfer Architecture with Exceptionally Long Lived Triplet State for Upconversion. *Chem. - Eur. J.* **2020**, *26*, 14912–14918.
- (106) Awwad, N.; Bui, A. T.; Danilov, E. O.; Castellano, F. N. Visible-Light-Initiated Free-Radical Polymerization by Homomolecular Triplet-Triplet Annihilation. *Chem* **2020**, *6*, 3071–3085.
- (107) Pun, A. B.; Sanders, S. N.; Sfeir, M. Y.; Campos, L. M.; Congreve, D. N. Annihilator Dimers Enhance Triplet Fusion Upconversion. *Chem. Sci.* **2019**, *10*, 3969–3975.
- (108) Nishimura, N.; Gray, V.; Allardice, J. R.; Zhang, Z.; Pershin, A.; Beljonne, D.; Rao, A. Photon Upconversion from Near-Infrared to Blue Light with TIPS-Anthracene as an Efficient Triplet-Triplet Annihilator. *ACS Mater. Lett.* **2019**, *1*, 660–664.
- (109) Zhou, Y.; Castellano, F. N.; Schmidt, T. W.; Hanson, K. On the Quantum Yield of Photon Upconversion via Triplet-Triplet Annihilation. *ACS Energy Lett.* **2020**, *5*, 2322–2326.
- (110) Arias-Rotondo, D. M. The Fruit Fly of Photophysics. *Nat. Chem.* **2022**, *14*, 716.
- (111) Schmid, L.; Kerzig, C.; Prescimone, A.; Wenger, O. S. Photostable Ruthenium(II) Isocyanoborato Luminophores and Their Use in Energy Transfer and Photoredox Catalysis. *JACS Au* **2021**, *1*, 819–832.
- (112) Bilger, J. B.; Kerzig, C.; Larsen, C. B.; Wenger, O. S. A Photorobust Mo(0) Complex Mimicking  $[\text{Os}(\text{2,2'}\text{-Bipyridine})_3]^{2+}$  and Its Application in Red-to-Blue Upconversion. *J. Am. Chem. Soc.* **2021**, *143*, 1651–1663.
- (113) Gimeno, L.; Phelan, B. T.; Sprague-Klein, E. A.; Roisnel, T.; Blart, E.; Gourlaouen, C.; Chen, L. X.; Pellegrin, Y. Bulky and Stable Copper(I)-Phenanthroline Complex: Impact of Steric Strain and Symmetry on the Excited-State Properties. *Inorg. Chem.* **2022**, *61*, 7296–7307.
- (114) Kim, D.; Teets, T. S. Strategies for Accessing Photosensitizers with Extreme Redox Potentials. *Chem. Phys. Rev.* **2022**, *3*, No. 021302.
- (115) Braun, J. D.; Lozada, I. B.; Kolodziej, C.; Burda, C.; Newman, K. M. E.; van Lierop, J.; Davis, R. L.; Herbert, D. E. Iron(II) Coordination Complexes with Panchromatic Absorption and Nano-second Charge-Transfer Excited State Lifetimes. *Nat. Chem.* **2019**, *11*, 1144–1150.
- (116) Carey, M. C.; Adelman, S. L.; McCusker, J. K. Insights into the Excited State Dynamics of Fe(II) Polypyridyl Complexes from Variable-Temperature Ultrafast Spectroscopy. *Chem. Sci.* **2019**, *10*, 134–144.
- (117) Dierks, P.; Vukadinovic, Y.; Bauer, M. Photoactive Iron Complexes: More Sustainable, but Still a Challenge. *Inorg. Chem. Front.* **2022**, *9*, 206–220.
- (118) Cagan, D. A.; Bim, D.; Silva, B.; Kazmierczak, N. P.; McNicholas, B. J.; Hadt, R. G. Elucidating the Mechanism of Excited-State Bond Homolysis in Nickel-Bipyridine Photoredox Catalysts. *J. Am. Chem. Soc.* **2022**, *144*, 6516–6531.
- (119) Zhang, Y.; Lee, T. S.; Favale, J. M.; Leary, D. C.; Petersen, J. L.; Scholes, G. D.; Castellano, F. N.; Milsmann, C. Delayed Fluorescence from a Zirconium(IV) Photosensitizer with Ligand-to-Metal Charge-Transfer Excited States. *Nat. Chem.* **2020**, *12*, 345–352.
- (120) Gowda, A. S.; Lee, T. S.; Rosko, M. C.; Petersen, J. L.; Castellano, F. N.; Milsmann, C. Long-Lived Photoluminescence of Molecular Group 14 Compounds through Thermally Activated Delayed Fluorescence. *Inorg. Chem.* **2022**, *61*, 7338–7348.
- (121) London, H. C.; Pritchett, D. Y.; Pienkos, J. A.; Mcmillen, C. D.; Whittemore, T. J.; Bready, C. J.; Myers, A. R.; Vieira, N. C.;

Harold, S.; Shields, G. C.; Wagenknecht, P. S. Photochemistry and Photophysics of Charge-Transfer Excited States in Emissive  $d^{10}/d^0$  Heterobimetallic Titanocene Tweezer Complexes. *Inorg. Chem.* **2022**, *61*, 10986–10998.

(122) Harris, J. P.; Reber, C.; Colmer, H. E.; Jackson, T. A.; Forshaw, A. P.; Smith, J. M.; Kinney, R. A.; Telser, J. Near-Infrared  $^2E_g \rightarrow ^4A_{2g}$  and Visible LMCT Luminescence from a Molecular Bis-(Tris(Carbene)Borate) Manganese(IV) Complex. *Can. J. Chem.* **2017**, *95*, 547–552.

(123) Chábera, P.; Liu, Y.; Prakash, O.; Thyrrhaug, E.; Nahhas, A. E.; Honarfar, A.; Essén, S.; Fredin, L. A.; Harlang, T. C. B.; Kjær, K. S.; Handrup, K.; Ericson, F.; Tatsuno, H.; Morgan, K.; Schnadt, J.; Häggström, L.; Ericsson, T.; Sobkowiak, A.; Lidin, S.; Huang, P.; Styring, S.; Uhlig, J.; Bendix, J.; Lomoth, R.; Sundström, V.; Persson, P.; Wärnmark, K. A Low-Spin Fe(III) Complex with 100-ps Ligand-to-Metal Charge Transfer Photoluminescence. *Nature* **2017**, *543*, 695–699.

(124) Kjær, K. S.; Kaul, N.; Prakash, O.; Chábera, P.; Rosemann, N. W.; Honarfar, A.; Gordivska, O.; Fredin, L. A.; Bergquist, K. E.; Häggström, L.; Ericsson, T.; Lindh, L.; Yartsev, A.; Styring, S.; Huang, P.; Uhlig, J.; Bendix, J.; Strand, D.; Sundström, V.; Persson, P.; Lomoth, R.; Wärnmark, K. Luminescence and Reactivity of a Charge-Transfer Excited Iron Complex with Nanosecond Lifetime. *Science* **2019**, *363*, 249–253.

(125) Pal, A. K.; Li, C.; Hanan, G. S.; Zysman-Colman, E. Blue-Emissive Cobalt(III) Complexes and Their Use in the Photocatalytic Trifluoromethylation of Polycyclic Aromatic Hydrocarbons. *Angew. Chem.* **2018**, *130*, 8159–8163.

(126) Wittwer, B.; Dickmann, N.; Berg, S.; Leitner, D.; Tesi, L.; Hunger, D.; Gratzl, R.; van Slageren, J.; Neuman, N. I.; Munz, D.; Hohloch, S. A Mesoionic Carbene Complex of Manganese in Five Oxidation States. *Chem. Commun.* **2022**, *58*, 6096–6099.

(127) Kaufhold, S.; Rosemann, N. W.; Chábera, P.; Lindh, L.; Bolaño Losada, I.; Uhlig, J.; Pascher, T.; Strand, D.; Wärnmark, K.; Yartsev, A.; Persson, P. Microsecond Photoluminescence and Photoreactivity of a Metal-Centered Excited State in a Hexacarbene-Co(III) Complex. *J. Am. Chem. Soc.* **2021**, *143*, 1307–1312.

(128) Kitzmann, W. R.; Moll, J.; Heinze, K. Spin-Flip Luminescence. *Photochem. Photobiol. Sci.* **2022**, *21*, 1309–1331.

(129) Otto, S.; Dorn, M.; Förster, C.; Bauer, M.; Seitz, M.; Heinze, K. Understanding and Exploiting Long-Lived near-Infrared Emission of a Molecular Ruby. *Coord. Chem. Rev.* **2018**, *359*, 102–111.

(130) Dorn, M.; Kalmbach, J.; Boden, P.; Kruse, A.; Dab, C.; Reber, C.; Niedner-Schatteburg, G.; Lochbrunner, S.; Gerhards, M.; Seitz, M.; Heinze, K. Ultrafast and Long-Time Excited State Kinetics of an NIR-Emissive Vanadium(III) Complex I: Synthesis, Spectroscopy and Static Quantum Chemistry. *Chem. Sci.* **2021**, *12*, 10780–10790.

(131) Doistau, B.; Jiménez, J. R.; Lawson Daku, L. M.; Piguet, C. Complex-as-Ligand Strategy as a Tool for the Design of a Binuclear Nonsymmetrical Chromium(III) Assembly: Near-Infrared Double Emission and Intramolecular Energy Transfer. *Inorg. Chem.* **2022**, *61*, 11023–11031.

(132) Bürgin, T. H.; Glaser, F.; Wenger, O. S. Shedding Light on the Oxidizing Properties of Spin-Flip Excited States in a  $Cr^{III}$  Polypyridine Complex and Their Use in Photoredox Catalysis. *J. Am. Chem. Soc.* **2022**, *144*, 14181–14194.

(133) Fulmer, G. R.; Miller, A. J. M.; Sherden, N. H.; Gottlieb, H. E.; Nudelman, A.; Stoltz, B. M.; Bercaw, J. E.; Goldberg, K. I. NMR Chemical Shifts of Trace Impurities: Common Laboratory Solvents, Organics, and Gases in Deuterated Solvents Relevant to the Organometallic Chemist. *Organometallics* **2010**, *29*, 2176–2179.